Figure 4. HCV core protein inhibits DDX3 promotion of IPS-1-mediated IFN-beta induction. (A) Expression plasmids for IPS-1 (100 ng), DDX3 (200 ng) and/or HCVO core (50 or 100 ng) were transfected into HEK293 cells in 24-well plates with reporter plasmids, and reporter activity was examined. (B) Expression plasmids for IPS-1 (100 ng), DDX3 (100 ng), and/or HCVO or JFH1 core (10, 25, 50 or 100 ng) were transfected into HEK293 cells, and reporter gene expression was analyzed. (C) IPS-1-, IKKepsilon- or NAP1-expressing plasmids were transfected into HEK293 cells with HCV JFH1 core-expressing plasmids (25 or 100 ng), for reporter gene analysis. (D) Plasmids for expression of FLAG-tagged IPS-1 (400 ng), HA-tagged DDX3 partial fragment (400 ng) and HCVO or JFH1 core (400 ng) were transfected into HEK293FT cells. 24 hrs later cells were lyzed and the lysate was incubated with anti-HA Ab for immunoprecipitation. The DDX3 (224-662)-bound IPS-1 was blotted onto a sheet and probed with anti-Flag Ab. Whole cell lysate was also stained with anti-tag Abs. (E) IPS-1 (100 ng), DDX3 (100 ng), JFH1 core (50 ng) and/or p125 luc reporter (100 ng) plasmids were transfected with HEK293 cells, with HCV 3'UTR poly-U/UC (PU/UC) RNA (25 ng), synthesized *in vitro*. Cell lysates were prepared after 24 hrs, and luciferase activities measured. One representative of at least three independent experiments is shown except for panel D, which is a representative of two sets of the experiments.
doi:10.1371/journal.pone.0014258.g004

amount of DNA was kept constant by adding empty vector. After 24 hrs, cells were fixed with 3% of paraformaldehyde in PBS for 30 minutes, and then permeabilized with PBS containing 0.2% of Triton X-100 for 15 min. Permeabilized cells were blocked with PBS containing 1% BSA, and were labeled with anti-Flag M2 mAb (Sigma) or anti-HA pAb (Sigma) in 1% BSA/PBS for 1 hr at room temperature [25]. In some cases, endogenous proteins were directly stained with anti-core (C7-50) mAb (Affinity BioReagents, Inc) or anti-DDX3 pAbs (Abcam, Cambridge MA). The cells were then washed with 1% BSA/PBS and treated for 30 min at room temperature with Alexa-conjugated antibodies (Molecular Probes). Thereafter, micro-cover glass was mounted onto slide glass using PBS containing 2.3% DABCO and 50% of glycerol. The stained cells were visualized at ×60 magnification under a FLUOVIEW (Olympus, Tokyo, Japan).

Results

DDX3 binds RNA species

We have performed proteome analyses of RNA-binding fractions in human dendritic cell lysate eluted from polyU and polyI:C Sepharose. 127 cytoplasmic proteins were reproducibly identified as polyI:C-binding proteins (Watanabe and Matsumoto, unpublished data). Four of them are DEAD/H box helicases. In this setting, we found DDX3 is a RNA-binding protein (Fig. 1A). DDX3 in cell lysate bound both polyU and polyI:C, while the control PKR bound only to polyI:C.

Using biotinylayed dsRNA, RNA-binding properties of DDX3 and RIG-I were tested by pull-down assay. DDX3 or RIG-I protein was co-precipitated with dsRNA in HEK293 cells expressing either alone of DDX3 or RIG-I (Fig. 1B). Strikingly, higher amounts of DDX3 and RIG-I were precipitated with dsRNA in cells expressing both proteins (Fig. 1B). This, taken together with previous results [11,14,16], indicates that DDX3 assembles in some RNA, RIG-I, IPS-1 and HCV core protein in its C-terminal domain (Fig. S1).

PolyU/UC but not replicon enhances IFN-β induction via IPS-1/DDX3

A polyU/UC sequence is present in the 3'-region of the HCV genome, and serves as a ligand for RIG-I in IPS-1 pathway activation [23]. We produced the polyU/UC RNA and tested its IFN-beta-inducing activity in the presence or absence of DDX3 and IPS-1 (Fig. 2A). HCV polyU/UC promoted IPS-1-mediated IFN-beta induction, and this was further enhanced by forced expression of DDX3/IPS-1 (Fig. 2A). Similar results were obtained with wild-type mouse embryonic fibroblasts (MEF) (Fig. 2B). We also investigated whether DDX3 enhanced IPS-1-mediated IFN-β promoter activation in a RIG-I −/− MEF background (Fig. 2B). In IPS-1/DDX3-expressing MEF cells, polyU/UC IFN-induction was almost totally abrogated by the lack of RIG-I, suggesting that the trace RIG-I protein in the IPS-1 complex is required for DDX3 enhancement of the polyU/UC-mediated IFN response.

DDX3 mRNA (Fig. 2C) and protein [11] were depleted in HEK293 cells by gene silencing with si-1 siRNA, so this was used for DDX3 loss-of-function analysis. Control or DDX3-silinced cells were transfected with increasing amounts of polyU/UC and IFN-beta promoter activation was determined by luciferase assay. DDX3 loss-of-function resulted in a decrease of promoter activation by intrinsic polyU/UC (Fig. 2D). The result was confirmed with cells over-expressing RIG-I and exogenous polyI:C stimulation. HEK293 cells were transfected with a plasmid for the expression of RIG-I and stimulated with polyI:C, an activator of the IPS-1 pathway (Fig. S2A). IFN-beta reporter activation was suppressed in si-1-treated cells that expressed RIG-I, since polyI:C lots often contain short size duplexes that can activate RIG-I [26]. In addition, DDX3 augmented the IFN-beta response in cells expressing MDA5/IPS-1 (Fig. S2B). Thus, DDX3 was also crucial for IPS-1-mediated IFN-beta promoter activation.

We next determined whether the HCV replicon triggers IPS-1/DDX3 IFN promoter activation, using human hepatocyte lines with the HCV replicon (O cells) or without it (Oc cells). In O cells with the HCV replicon, IPS-1/DDX3 expression showed minimal enhancement of IFN-beta promoter activation (Fig. 3A), while in control Oc cells with no replicon, DDX3 facilitated IFN-beta promoter activation (Fig. 3B). Similarly, an augmented IFN promoter response to polyU/UC was observed in control Oc cells, but not in O cells (Figs. 3C and 3D). HCV RNA was prepared from O cells, and its ability to activate the IFN-beta reporter was tested in HEK293 cells (Fig. 3E). The HCV RNA of O cells had a high potency to induce reporter activation, and this activity was largely abrogated by si-1 siRNA treatment. Therefore, DDX3 augments IPS-1-mediated IFN-beta promoter activation in hepatocyte O cells, and HCV RNA, presumably the 3'UTR, participates in this induction. However, no IFN-beta reporter activation was detected in O cells which harbor HCV replicon. Therefore, an unidentified viral factor appeared to participate in suppressing virus RNA-mediated IFN-beta induction, which occurred in O cells overexpressing DDX3/IPS-1.

HCV core protein inhibits IPS-1 signaling through DDX3

What HCV proteins participate in IFN-beta induction was tested in a pilot study using protein expression analysis. We found that expression of HCV core protein as well as NS3/4A led to suppression of IFN-beta reporter activity in Oc cells (data not shown). The HCV core protein physically binds DDX3 [14,16], and co-localizes with DDX3 in the cytoplasm of HeLa cells transfected with HCV core protein [14]. Furthermore, we showed that DDX3 binds IPS-1, which resides on the mitochondrial outer membrane, and assembles into RNA-sensing receptors. Since some populations of the HCV core protein localize on the mitochondrial outer membrane [27], we tested if HCV core

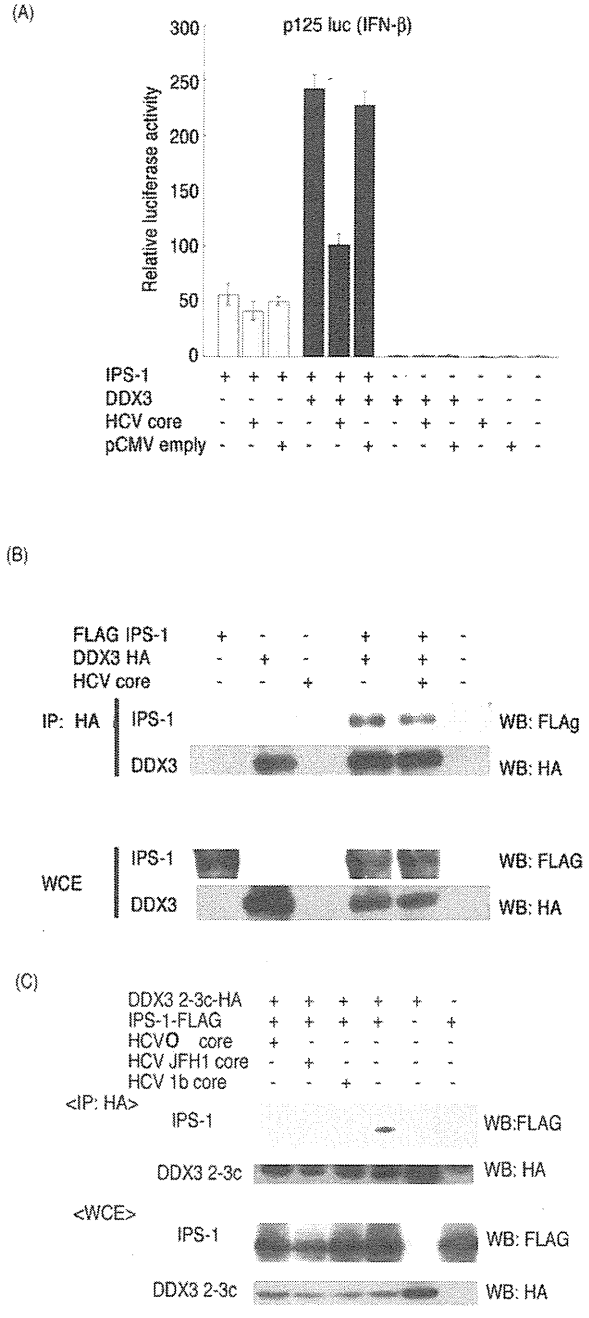

Figure 5. Properties of a 1b-type core protein in the IPS-1 pathway. (A) A core protein derived from an HCV patient suppressed DDX3-mediated activation of IPS-1 signaling. The 1b-type core protein was cloned into the pCMV vector from a patient with hepatitis C. IPS-1 (100 ng), DDX3 (100 ng) and HCV core (100 ng) expression vectors were transfected into HEK293 cells with a reporter plasmid (p125luc), for analysis as in Figure 4. (B) The core protein reduced interaction between full-length DDX3 and IPS-1. The plasmids encoding core protein (400 ng), DDX3-HA (400 ng) and FLAG-IPS-1 (400 ng) were transfected into HEK293FT cells. After 24 hrs, cell lysates were prepared and immunoprecipitation was carried out using anti-HA (DDX3-HA). (C) The core protein blocked interaction between the C-terminal fragment of DDX3 and IPS-1. The C-terminal region of DDX3 (199–662 aa) called DDX3 2-3c, IPS-1, HCV (O) and JFH1 or 1b core expression plasmids were transfected into HEK293FT cells. After 24 hrs, cell lysates were prepared and immunoprecipitation was carried out with anti-HA (DDX3 2–3c). Immunoprecipitates were analyzed by SDS-PAGE and Western blotting with anti-HA or FLAG antibodies. The results are representative of two independent experiments.
doi:10.1371/journal.pone.0014258.g005

protein affects IPS-1 signaling by binding to DDX3. The cDNAs for HCV core proteins, genotype 1b (HCVO) and 2a (JFH1) [16], were co-transfected into HEK293 together with IPS-1, DDX3, and reporter plasmids, and core protein interference with IPS-1/DDX3-mediated IFN-beta promoter activation was examined. We found that the core proteins of HCVO and JFH1 suppressed IPS-1/DDX3-augmented IFN-beta-induction in a dose-dependent manner (Fig. 4A and 4B). Without DDX3 transfection, core protein had no effect on IPS-1-mediated IFN-beta promoter activation (Fig. 4A). JFH1 core slightly more efficiently inhibited IPS-1/DDX3-augmented IFN-beta-induction than HCVO core (Fig. 4B).

Although some endogenous DDX3 was present in the cytoplasm without DDX3 transfection, only IPS-1 transfection permitted minimal induction of IFN-beta. It is notable that high doses of the HCV JFH1 core protein was needed to inhibit the IPS-1-mediated IFN-beta-induction signal (Fig. 4C, left panel). Since the imaging profile of DDX3 is not always monotonous in human cells, its distribution may be biased in the cytoplasm, which may reason that only a high dose of HCV core involves preoccupied DDX3 protein to inhibit the IPS-1 pathway. This is consistent with earlier reports on an NS3-independent mechanism to block IFN induction using HCV-infected Huh 7 cells [28].

IPS-1 transduces a RNA replication signal to result in IFN-beta output using downstream proteins, such as NAP1 and IKKεsilon. If the HCV core protein interferes with IPS-1 function through DDX3, the core should not inhibit over-expressed downstream molecules. As predicted, HCV core protein did not suppress the IKKεpsilon- or NAP1-mediated IFN-beta-inducing signal (Fig. 4C, center and right panels). Hence, the core protein blocks the action of endogenous DDX3 and overexpressed IPS-1 to facilitate minimal IFN-beta promoter activation, and this IFN-beta blocking function of core does not target IKKεpsilon or NAP1 (Fig. 4C). An upstream molecule of IKKεpsilon and NAP1 is predicted to be the target of the HCV core protein, which is in line with the fact that the HCV core protein interacts with DDX3 [14,16].

To further confirm this model, we examined whether the HCV core protein inhibits the physical interaction between IPS-1 and DDX3. Full length IPS-1 and the C-terminal fragment of DDX3, which binds to the IPS-1 CARD-like region, were transfected into HEK293 cells, with or without the HCV core protein, and the DDX3 fragment was immunoprecipitated. Expression of HCV core proteins strongly inhibited interaction between the DDX3 C-terminal fragment and IPS-1 (Fig. 4D). JFH1 core appeared to show greater inhibition to DDX3-IPS-1 interaction than HCVO. We then examined this IFN-beta blocking function of JFH1 core in a similar cell condition plus polyU/UC. DDX3/IPS-1-enhanced p125luc reporter activity in cells stimulated with polyU/UC (Fig. 4E) was decreased in cells expressing HCV core. The results suggest that the role of the core in HCV-infected cells is to remove DDX3 from IPS-1, and facilitate its interaction with HCV replication complex (Fig. S1).

PolyU/UC HCV RNA activates the IFN-beta promoter (Fig. 2A), and this activity was inhibited by expression of the HCV core protein (Fig. 4E). PolyI:C/RIG-I-mediated IFN-β promoter activation was similarly suppressed by the core protein

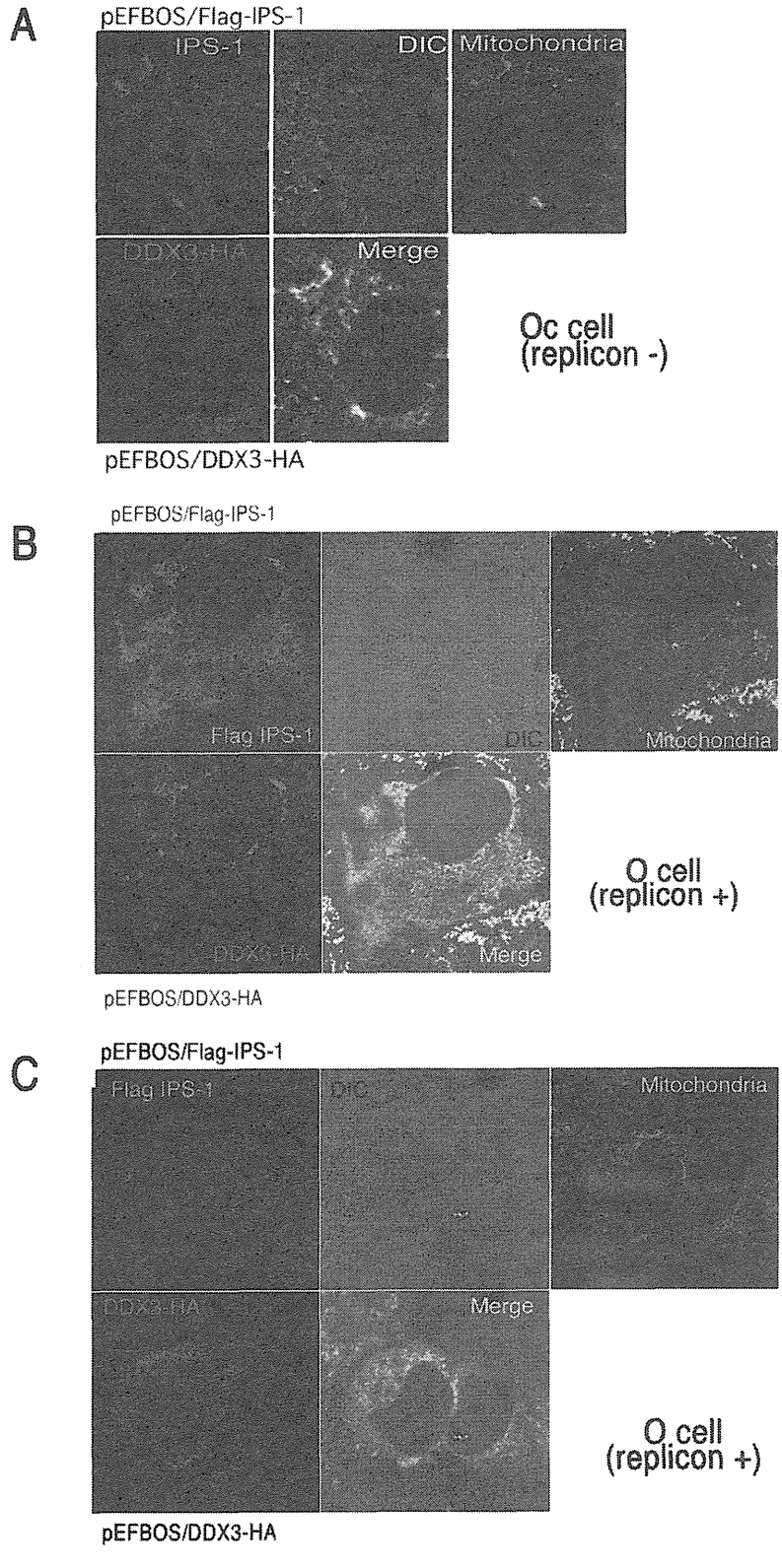
A
pEFBOS/Flag-IPS-1
IPS-1
DIC
Mitochondria
DDX3-HA
Merge
Oc cell
(replicon -)
pEFBOS/DDX3-HA
B
pEFBOS/Flag-IPS-1
Flag IPS-1
DIC
Mitochondria
DDX3-HA
Merge
O cell
(replicon +)
pEFBOS/DDX3-HA
C
pEFBOS/Flag-IPS-1
Flag IPS-1
DIC
Mitochondria
DDX3-HA
Merge
O cell
(replicon +)
pEFBOS/DDX3-HA

Figure 6. Distribution of DDX3 and IPS-1. (A) DDX3 colocalizes with IPS-1 on the mitochondria in Oc cells. HA-tagged DDX3 and FLAG-tagged IPS-1 were co-transfected into Oc cells. After 24 hrs, cells were fixed with formaldehyde and stained with anti-HA polyclonal and FLAG monoclonal Abs. Alexa488 (DDX3-HA) or Alexa633 antibody was used for second antibody. Mitochondria were stained with Mitotracker Red. Similar IPS-1-DDX3 merging profiles were observed in Huh7.5.1 cells (Fig. S3). (B,C) O cells with the HCV replicon poorly formed the DDX3-IPS-1 complex. Plasmids carrying IPS-1 (100 ng) or DDX3 (150 or 300 ng) were transfected into O (HCV replicon +) as in Oc cells (no replicon, panel A). After 24 hrs, localization of IPS-1 and DDX3 was examined by confocal microscopy. Two representatives which differ from the conventional profile (as in panel A) are shown. Similar sets of experiments were performed four times to confirm the results.
doi:10.1371/journal.pone.0014258.g006

(Fig. S2A). MDA5-dependent IFN-beta promoter activation was also suppressed by the core expression (Fig. S2B). The inhibitory effect of the core protein on DDX3-IPS-1 interaction was further confirmed using an 1b core isoform isolated from a patient. This HCV core protein also reduced interaction as well as IPS-1-mediated IFN-beta promoter activation (Fig. 5A). The blocking effect was relatively weak in cells expressing IPS-1 and full-length DDX3 (Fig. 5B). We presume that this is because there are multiple binding sites for IPS-1 in the DDX3 whole molecule [11]. For binding assay, we used DDX3 2-3c (across a.a. 199~662, longer than 224~662) instead of the whole DDX3. In fact, DDX3(199-662)-IPS-1 interaction was blocked by the additional expression of core protein (HCVO, JFH1 or 1b core) in Fig. 5C. Ultimately, HCV core protein suppresses IPS-1 signaling by blocking the interaction between the C-terminal region of DDX3 and the CARD-like region of IPS-1, and this inhibition apparently causes the disruption of the active RIG-I/DDX3/IPS-1 complex that efficiently induces IFN-beta production signaling.

Localization of DDX3 and HCV core protein in O cells

We attempted to confirm this finding by tag-expressed proteins and imaging analysis. In Huh7.5 cells IPS-1 colocalized with DDX3 around the mitochondria (Fig. S3), and so did in the hepatocyte lines Oc cells with no HCV replicon (Fig. 6A). In Oc and Huh7.5.1 cells with no HCV replicon, abnormal distribution of IPS-1 was barely observed (Fig. 6A, Fig. S3). In O cells expressing DDX3 and IPS-1, by contrast, two distinct profiles of IPS-1 were observed in addition to the Fig. 6A pattern of IPS-1: diminution or spreading of the IPS-1 protein over mitochondria (Fig. 6B,C). IPS-1 may be degraded by NS3/4A in some replicon-expressing O cells as reported previously [5,28]. We counted number of cells having the pattern represented by Fig. 6 panel B and those similar to Fig. 6 panel C, and in most cases the latter patterns were predominant.

What happens in the O cells with replicon when the core protein is expressed was next tested. Using O and Oc cells, we tested the localization of the core protein and DDX3 in comparison with IFN-inducing properties (Fig. 3). In O cells with full-length HCV replicon, DDX3 was localized proximal to the lipid droplets (LD) (Fig. 7A top panel) around which HCV particles assembled [29]. HCV core protein and DDX3 were partly colocalized in the HCV replicon-expressing cells (Fig. 7A center panel). The results were confirmed with HCV replicon-expressing O cells where endogenous core and DDX3 were stained (Fig. 7B upper panel). Partial merging between core and DDX3 was reproduced in this case, too. In contrast, sO cells, which possess a subgenomic replicon lacking the cording region of the core protein, showed no merging profile of DDX3 and LD (Fig. 7A bottom panel). Likewise, Oc cells barely formed assembly consisting of LD (where the core assembles) and overexpressed DDX3 (Fig. 7A bottom panel) or endogenous DDX3 (Fig. 7B lower panel). O cells expressing DDX3 tended to form large spots compared to Oc cells (with no replicon) and sO cells (core-less replicon) with DDX3.

Overexpressed DDX3 allowed the Oc cells to induce IPS-1-mediated IFN-beta promoter activation (Fig. 3B), while this failed to happen in O cells having HCV replicon (Fig. 3A). Ultimately, overexpressed IPS-1 did not facilitate efficient merging with DDX3 in O cells with replicon (Fig. 6B,C) compared to Oc cells or Huh7.5 cells with no replicon (Fig. 6A, Fig. S3). The results on the functional and immnoprecipitation analyses, together with the imaging profiles, infer that the IPS-1-enhancing function of DDX3 should be blocked by both NS3/4A-mediated IPS-1 degradation and the HCV core which translocates DDX3 from the IPS-1 complex to the proximity of LD in HCV replicon-expressing cells.

Discussion

We investigated the effect of the HCV core protein on the cytosolic DDX3 that forms a complex with IPS-1 to enhance the RIG-I-mediated RNA-sensing pathway. We demonstrated that the core protein removes DDX3 from the IFN-β-inducing complex, leading to suppression of IFN-β induction. DDX3 is functionally complex, since its protective role against viruses may be modulated by the synthesis of viral proteins. DDX3 acts on multiple steps in the IFN-inducing pathway [30]. In addition, DDX3 interacts with the HCV core protein in HCV-infected cells and promotes viral replication [16]. This alternative function is accelerated by the HCV core protein, resulting in augmented HCV propagation [14,16]. More recently, Patal et al., reported that interaction of DDX3 with core protein is not critical for the support of viral replication by DDX3, although DDX3 and core protein colocalize with lipid droplet [15]. If this is the case, what function is revealed by the interaction between DDX3 and HCV core protein remain unsettled. At least, HCV replication is not blocked by this molecular interaction [15].

It remains unclear in Fig. 4C why higher doses of JFH1 core protein are required to inhibit enhancement of IPS-1 signaling by endogenous DDX3 than by exogenously overexpressed DDX3. One possibility is that endogenous DDX3 is preoccupied in a molecular complex other than the IPS-1 pathway since DDX3 is involved in almost every step of RNA metabolism and its localization affects its functional profile [18,30].

Together with these findings, the results presented here suggest that the HCV core inactivates IPS-1 in a mode different from NS3/4A [5,31]. The core protein may switch DDX3 from an antiviral mode to an HCV propagation mode. The core protein localizes to the N-terminus of the HCV translation product, and is generated in infected cells before NS3/4A proteolytically liberates non-structural proteins and inactivates IPS-1. Our results on how the HCV core protein interferes with the interaction between DDX3 and IPS-1 add several possibilities to notions about the HCV function on the IFN-beta-inducing pathway [18].

DDX3 appears to be a prime target for viral manipulation, since at least three different viruses, including HCV [14], Hepatitis B virus [32], and poxviruses [8], encode proteins that interact with DDX3 and modulate its function. These viruses seem to co-opt DDX3, and also require it for replication. The viruses are all oncogenic, and may confer oncogenic properties to DDX3.

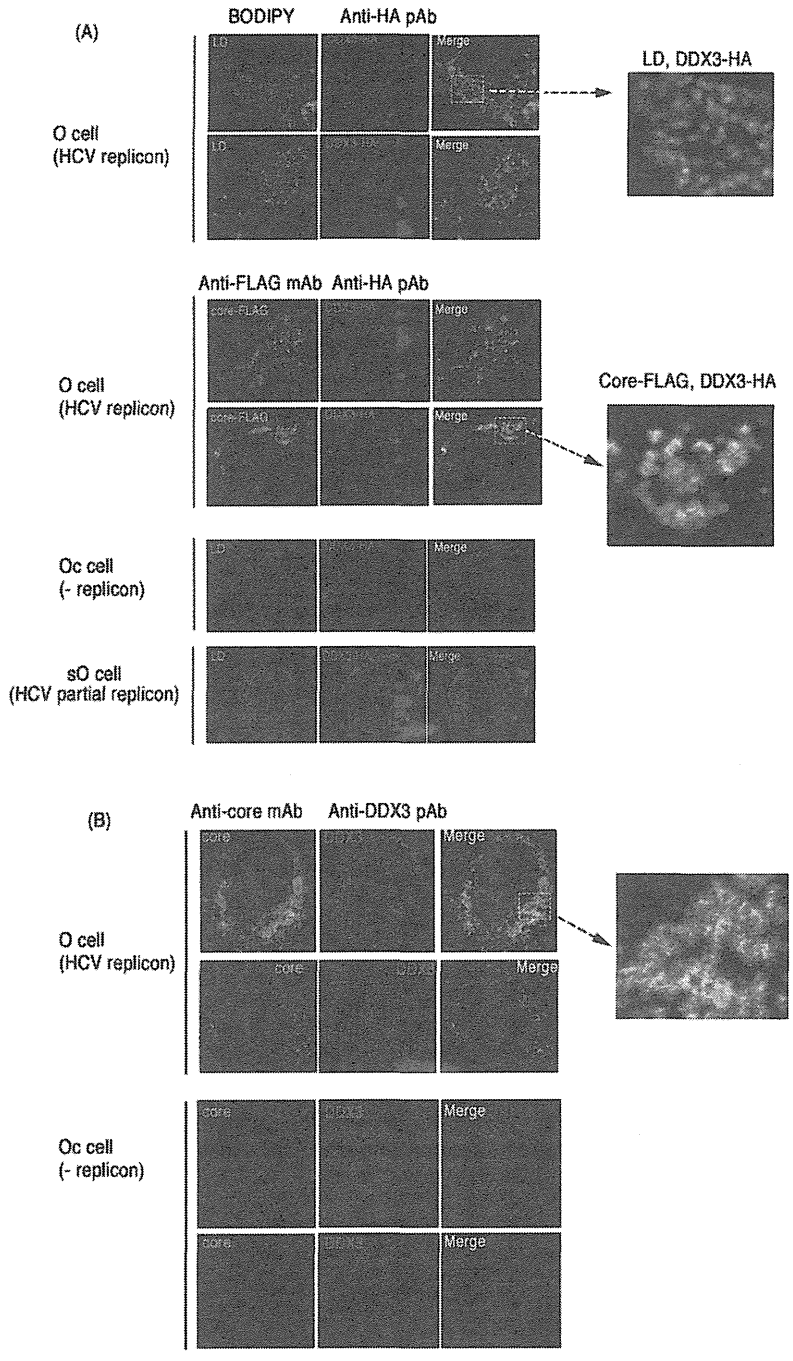

Figure 7. Partial association of endogenous and overexpressed DDX3 with HCV core protein in hepatocyte lines. (A) O cells with the HCV replicon form DDX3-containing speckles in the cytoplasm. O cells contain full-length HCV replicon, and Oc cells do not [16]. O cells were transfected with a plasmid expressing HA-tagged DDX3 (top panel). In other experiments, O cells were transfected with plasmids expressing HA-tagged DDX3 and FLAG-tagged HCV core protein (center panel). After 24 hrs, cells were stained with anti-HA or FLAG antibodies. Proteins were visualized with Alexa488 or 564 second antibodies and the LD was stained with BODIPY493/503. In the bottom panel, Oc cells (no replicon) and sO cells with the core-less subgenomic replicon [16] were transfected with a plasmid expressing HA-tagged DDX3. After 24 hrs, cells were stained with anti-HA antibodies. LD was stained with BODIPY493/503. (B) Endogenous DDX3-HCV core association in O cells. O or Oc cells were cultured to amplify the HCV replicon. Cells were stained with anti-core mAb and anti-DDX3pAb and secondary antibodies. Similar sets of experiments were performed three times to confirm the results.
doi:10.1371/journal.pone.0014258.g007

DDX3 is also involved in human immunodeficiency virus RNA translocation [33]. The DDX3 gene is conserved among eukaryotes, and includes the budding yeast homolog, Ded1 [34]. The Ded1 helicase is essential for initiation of host mRNA translation, and human DDX3 complements the lethality of Ded1 null yeast [14,35]. Another function of DDX3 is to bind viral RNA to modulate RNA replication and translocation. Constitutive expression of the HCV core or other DDX3-binding proteins may impede IFN induction and promote cell cycle progression. These reports are consistent with the implication of DDX3 in various steps of RNA metabolism in cells that contain both host and viral RNAs.

A continuing question is the physiological role of the molecular complex of DDX3 and IPS-1 during replication of HCV in hepatocytes. HCV proteins generated in host hepatocytes usually induce an HCV-permissive state in patients, for example in the IFN-inducing pathways. NS3/4A protease induces rapid degradation of IPS-1 [5,31] and TICAM-1/TRIF [36]. NS5A interferes with the MyD88 function [37]. Viral replication ultimately blocks the STAT1-mediated IFN-amplification pathway [38]. PKR may be an additional factor by which HCV controls type I IFN production [39]. Our results add to our knowledge of the mechanism of how HCV circumvents IFN induction in host cells: HCV core protein suppresses the initial step of IFN-beta induction by interfering with DDX3-IPS-1 association. Indeed, the core protein functions as the earliest IFN suppressor, since it is generated first in HCV-infected cells, and rapidly couples with DDX3 to retract it from the IPS-1 complex, resulting in localization of DDX3 near the LD (Fig. 7). It is HCV that hijacks this protein for establishing infection. Although gene disruption of DDX3 makes mice lethal, this issue will be further tested using IPS-1 −/− hepatocytes expressing human CD81 and occludin [40], in which HCV replication would proceed.

DDX3 primarily is an accelerating factor for antiviral response through IPS-1-binding. Many host proteins other than DDX3 may positively regulate HCV replication in hepatocytes in association with the IPS-1 pathway. In this context, we know LGP2 [41] and STING [42] act as positive regulators in virus infection. Peroxisomes serve as signaling platforms for recruiting IPS-1 with a different signalosome than mitochondria [43]. It appears rational that HCV harbors strategies to circumvent these positive regulators in the relevant steps of the IFN-inducing pathway.

Imaging studies suggest that the complex of IPS-1 involving the membrane of mitochondrial/peroxisomes differ from that free from the membrane. Although IPS-1 is liberated from the membrane by NS3/4A having largely intact cytosolic domain, it loses the IFN-inducing function [5,31]. Our results could offer the possibility that the clipped-out form of IPS-1 immediately fails to form the conventional complex for IRF-3 activation any more [44] or is easily degraded further to be inactive (Fig. 6C). Indeed, there are a number of mitochondria-specific molecules which assemble with IPS-1 [45]. Formation of the molecular complex on the mitochondria rather than simple association between IPS-1 and DDX3 may be critical for the DDX3 function.

Evidence is accumulating that HCV checks many steps in the IFN-inducing pathway throughout the early and late infection stages, and suppresses IFN production by multiple means. Disruption of IPS-1 function by both NS3/4A and core protein may be crucial in HCV-infected Huh7.5 cells, even though the cells harbor dysfunctional RIG-I [46]. Type I IFN suppresses tumors by causing expression of p53 and other tumor-suppressing agents [47]. These unique features of the HCV core protein require further confirmation, and should be minded in investigation of HCV persistency, chronic infection and progression to cirrhosis and carcinoma.

Supporting Information

Figure S1 The IPS-1 complex. IPS-1 and HCV core bind C-terminal regions of DDX3. DDX3 captures dsRNA at the C-terminal domain. This figure is constructed from [11], [14] and [16].
Found at: doi:10.1371/journal.pone.0014258.s001 (0.41 MB TIF)

Figure S2 DDX3 enhances RIG-I-mediated IFN-β promoter activation induced by polyI:C. (A) DDX3 si-1 or control siRNA was transfected into HEK293 cells with reporter plasmids and RIG-I-expression plasmid or control plasmid (100 ng). After 48 hrs, cells were stimulated with polyI:C (20 μg/ml) with dextran for 4 hrs, and activation of the reporter p125luc was measured. (B) MDA5 (25 ng), IPS-1 (100 ng), DDX3 (100 ng), JFH1 core (50 ng) and/or p125 luc reporter (100 ng) plasmids were transfected with HEK293 cells. Cell lysates were prepared after 24 hrs, and luciferase activities measured. The results are representative of two independent experiments, each performed in triplicate.
Found at: doi:10.1371/journal.pone.0014258.s002 (0.17 MB TIF)

Figure S3 DDX3 colocalizes with IPS-1 on the mitochondria in Huh7.5.1 cells. HA-tagged DDX3 and FLAG-tagged IPS-1 were co-transfected into Huh7.5.1 cells. After 24 hrs, cells were fixed with formaldehyde and stained with anti-HA polyclonal and FLAG monoclonal Abs. Alexa488 (DDX3-HA) or Alexa633 antibody was used for second antibody. Mitochondria were stained with Mitotracker Red. A representative result from three independent experiments is shown.
Found at: doi:10.1371/journal.pone.0014258.s003 (0.92 MB TIF)

Acknowledgments

We thank Drs. Y. Matsuura (Osaka Univ.), Kyoko Mori (Okayama Univ.), and M. Sasai (Yale Univ.) for invaluable discussions. Thanks are also due to Drs. T. Ebihara, K. Funami, A. Matsuo, A. Ishii, and M. Shingai in our laboratory for their critical discussions.

Author Contributions

Conceived and designed the experiments: HO MM TS. Performed the experiments: HO MM. Analyzed the data: HO MM KS TS. Contributed reagents/materials/analysis tools: MI AW OT SA NK KS. Wrote the paper: HO TS.

References

1. Yoneyama M, Kikuchi M, Natsukawa T, Shinobu N, Imaizumi T, et al. (2004) The RNA helicase RIG-I has an essential function in double-stranded RNA-induced innate antiviral responses. Nat Immunol 5: 730–737.
2. Yoneyama M, Kikuchi M, Matsumoto K, Imaizumi T, Miyagishi M, et al. (2005) Shared and unique functions of the DExD/H-box helicases RIG-I, MDA5, and LGP2 in antiviral innate immunity. J Immunol 175: 2851–2858.
3. Kato H, Takeuchi O, Sato S, Yoneyama M, Yamamoto M, et al. (2006) Differential roles of MDA5 and RIG-I helicases in the recognition of RNA viruses. Nature 441: 101–105.
4. Kawai T, Takahashi K, Sato S, Coban C, Kumar H, et al. (2005) IPS-1, an adaptor triggering RIG-I- and Mda5-mediated type I interferon induction. Nat Immunol 6: 981–988.

5. Meylan E, Curran J, Hofmann K, Moradpour D, Binder M, et al. (2005) Cardif is an adaptor protein in the RIG-I antiviral pathway and is targeted by hepatitis C virus. Nature 437: 1167–1172.
6. Seth RB, Sun L, Ea CK, Chen ZJ (2005) Identification and characterization of MAVS, a mitochondrial antiviral signaling protein that activates NF-kappaB and IRF 3. Cell 122: 669–682.
7. Xu LG, Wang YY, Han KJ, Li LY, Zhai Z, et al. (2005) VISA is an adapter protein required for virus-triggered IFN-beta signaling. Mol Cell 19: 727–740.
8. Schroder M, Baran M, Bowie AG (2008) Viral targeting of DEAD box protein 3 reveals its role in TBK1/IKKepsilon-mediated IRF activation. Embo J 27: 2147–2157.
9. Soulat D, Bürckstümmer T, Westermayer S, Goncalves A, Bauch A, et al. (2008) The DEAD-box helicase DDX3X is a critical component of the TANK-binding kinase 1-dependent innate immune response. Embo J 27: 2135–2146.
10. Kravchenko VV, Mathison JC, Schwamborn K, Mercurio F, Ulevitch RJ (2003) IKKi/IKKepsilon plays a key role in integrating signals induced by pro-inflammatory stimuli. J Biol Chem 278: 26612–26619.
11. Oshiumi H, Sakai K, Matsumoto M, Seya T (2010) DEAD/H BOX 3 (DDX3) helicase binds the RIG-I adaptor IPS-1 to up-regulate IFN-beta inducing potential. Eur J Immunol 40: 940–948.
12. Chao CH, Chen CM, Cheng PL, Shih JW, Tsou AP, et al. (2006) A DEAD box RNA helicase with tumor growth-suppressive property and transcriptional regulation activity of the p21waf1/cip1 promoter, is a candidate tumor suppressor. Cancer Res 66: 6579–6588.
13. Rocak S, Linder P (2004) DEAD-box proteins: the driving forces behind RNA metabolism. Nat Rev Mol Cell Biol 5: 232–241.
14. Owsianka AM, Patel AH (1999) Hepatitis C virus core protein interacts with a human DEAD box protein DDX3. Virology 257: 330–340.
15. Angus AGN, Dalrymple D, Boulant S, McGivern DR, Clayton RF, et al. (2010) Requirement of cellular DDX3 for hepatitis C virus replication is unrelated to its interaction with the viral core protein. J Gen Virol 91: 122–132.
16. Ariumi Y, Kuroki M, Abe K, Dansako H, Ikeda M, et al. (2007) DDX3 DEAD-box RNA helicase is required for hepatitis C virus RNA replication. J Virol 81: 13922–13926.
17. Chang PC, Chi CW, Chau GY, Li FY, Tsai YH, et al. (2006) DDX3, a DEAD box RNA helicase, is deregulated in hepatitis virus-associated hepatocellular carcinoma and is involved in cell growth control. Oncogene 25: 1991–2003.
18. Schroder M (2010) Human DEAD-box protein 3 has multiple functions in gene regulation and cell cycle control and is a prime target for viral manipulation. Biochem Pharmacol 79: 297–306.
19. Ikeda M, Abe K, Dansako H, Nakamura T, Naka K, et al. (2005) Efficient replication of a full-length hepatitis C virus genome, strain O, in cell culture, and development of a luciferase reporter system. Biochem Biophys Res Commun 329: 1350–1359.
20. Lin W, Kim SS, Yeung E, Kamegaya Y, Blackard JT, et al. (2006) Hepatitis C virus core protein blocks interferon signaling by interaction with the STAT1 SH2 domain. J Virol 2006 Sep; 80(18): 9226–35.
21. Sasai M, Shingai M, Funami K, Yoneyama M, Fujita T, et al. (2006) NAK-associated protein 1 participates in both the TLR3 and the cytoplasmic pathways in type I IFN induction. J Immunol 177: 8676–8683.
22. Oshiumi H, Matsumoto M, Funami K, Akazawa T, Seya T (2003) TICAM-1, an adaptor molecule that participates in Toll-like receptor 3-mediated interferon-beta induction. Nat Immunol 4: 161–167.
23. Saito T, Owen DM, Jiang F, Marcotrigiano J, Gale M, Jr. (2008) Innate immunity induced by composition-dependent RIG-I recognition of hepatitis C virus RNA. Nature 454: 523–527.
24. Saito T, Hirai R, Loo YM, Owen D, Johnson CL, et al. (2007) Regulation of innate antiviral defenses through a shared repressor domain in RIG-I and LGP2. Proc Natl Acad Sci U S A 104: 582–587.
25. Matsumoto M, Funami K, Tanabe M, Oshiumi H, Shingai M, et al. (2003) Subcellular localization of Toll-like receptor 3 in human dendritic cells. J Immunol 171: 3154–3162.
26. Oshiumi H, Matsumoto M, Hatakeyama S, Seya T (2009) Riplet/RNF135, a RING finger protein, ubiquitinates RIG-I to promote interferon-beta induction during the early phase of viral infection. J Biol Chem 284: 807–817.
27. Schwer B, Ren S, Pietschmann T, Kartenbeck J, Kaehlcke K, et al. (2004) Targeting of hepatitis C virus core protein to mitochondria through a novel C-terminal localization motif. J Virol 78: 7958–7968.
28. Cheng G, Zhong J, Chisari FV (2006) Inhibition of dsRNA-induced signaling in hepatitis C virus-infected cells by NS3 protease-dependent and -independent mechanisms. Proc Natl Acad Sci U S A 103: 8499–8504.
29. Miyanari Y, Atsuzawa K, Usuda N, Watashi K, Hishiki T, et al. (2007) The lipid droplet is an important organelle for hepatitis C virus production. Nat Cell Biol 9: 1089–1097.
30. Mulhern O, Bowie AG (2010) Unexpected roles for DEAD-box protein 3 in viral RNA sensing pathways. Eur J Immunol 40: 933–935.
31. Li XD, Sun L, Seth RB, Pineda G, Chen ZJ (2005) Hepatitis C virus protease NS3/4A cleaves mitochondrial antiviral signaling protein off the mitochondria to evade innate immunity. Proc Natl Acad Sci U S A 102: 17717–17722.
32. Wang H, Kim S, Ryu WS (2009) DDX3 DEAD-Box RNA helicase inhibits hepatitis B virus reverse transcription by incorporation into nucleocapsids. J Virol 83: 5815–5824.
33. Yedavalli VS, Neuveut C, Chi YH, Kleiman L, Jeang KT (2004) Requirement of DDX3 DEAD'box RNA helicase for HIV-1 Rev-RRE export function. Cell 119: 381–392.
34. Chuang RY, Weaver PL, Liu Z, Chang TH (1997) Requirement of the DEAD-Box protein ded1p for messenger RNA translation. Science 275: 1468–1471.
35. Mamiya N, Worman HJ (1999) Hepatitis C virus core protein binds to a DEAD box RNA helicase. J Biol Chem 274: 15751–15756.
36. Li K, Foy E, Ferreon JC, Nakamura M, Ferreon AC, et al. (2005) Immune evasion by hepatitis C virus NS3/4A protease-mediated cleavage of the Toll-like receptor 3 adaptor protein TRIF. Proc Natl Acad Sci U S A 102: 2992–2997.
37. Abe T, Kaname Y, Hamamoto I, Tsuda Y, Wen X, et al. (2007) Hepatitis C virus nonstructural protein 5A modulates the toll-like receptor-MyD88-dependent signaling pathway in macrophage cell lines. J Virol 81: 8953–8966.
38. Heim MH, Moradpour D, Blum HE (1999) Expression of hepatitis C virus proteins inhibits signal transduction through the Jak-STAT pathway. J Virol 73: 8469–8475.
39. Arnaud N, Dabo S, Maillard P, Budkowska A, Kalliampakou KI, et al. (2010) Hepatitic C virus controls interferon production through PKR activation. PLoS One 5: e10575.
40. Ploss A, Evans MJ, Gaysinskaya VA, Panis M, You H, et al. (2009) Human occludin is a hepatitis C virus entry factor required for infection of mouse cells. Nature 457: 882–886.
41. Satoh T, Kato H, Kumagai Y, Yoneyama M, Sato S, et al. (2010) LGP2 is a positive regulator of RIG-I- and MDA5-mediated antiviral responses. Proc Natl Acad Sci U S A 107: 1512–1517.
42. Ishikawa H, Ma Z, Barber GN (2009) STING regulates intracellular DNA-mediated, type I interferon-dependent innate immunity. Nature 461: 788–793.
43. Dixit E, Boulant S, Zhang Y, Lee ASY, Odendall C, et al. (2010) Peroxisomes are signaling platforms for antiviral innate immunity. Cell 141: 668–681.
44. Yasukawa K, Oshiumi H, Takeda M, Ishihara N, Yanagi Y, et al. (2009) Mitofusin 2 inhibits mitochondrial antiviral signaling. Sci Signal 2: ra47.
45. Scott I (2010) The role of mitochondria in the mammalian antiviral defense system. Mitochondrion 10: 316–320.
46. Binder M, Kochs G, Bartenschlager R, Lohmann V (2007) Hepatitis C virus escape from the interferon regulatory factor 3 pathway by a passive and active evasion strategy. Hepatology 46: 1365–1374.
47. Takaoka A, Yanai H, Kondo S, Duncan G, Negishi H, et al. (2005) Integral role of IRF-5 in the gene induction programme activated by Toll-like receptors. Nature 434: 243–249.

Published November 8, 2010

JEM

Article

Identification of a polyI:C-inducible membrane protein that participates in dendritic cell–mediated natural killer cell activation

Takashi Ebihara,[1] Masahiro Azuma,[1] Hiroyuki Oshiumi,[1] Jun Kasamatsu,[1] Kazuya Iwabuchi,[2] Kenji Matsumoto,[3] Hirohisa Saito,[3] Tadatsugu Taniguchi,[4] Misako Matsumoto,[1] and Tsukasa Seya[1]

[1]Department of Microbiology and Immunology, Hokkaido University Graduate School of Medicine, Kita-ku, Sapporo 060-8638, Japan
[2]Division of Immunobiology, Institute for Genetic Medicine, Hokkaido University, Sapporo, Japan, 060-0815, Japan
[3]Department of Allergy and Immunology, National Research Institute for Child Health and Development, Setagaya-ku, Tokyo 157-8535, Japan
[4]Department of Immunology, Graduate School of Medicine and Faculty of Medicine, University of Tokyo, Bunkyo-ku, Tokyo 113-0033, Japan

In myeloid dendritic cells (mDCs), TLR3 is expressed in the endosomal membrane and interacts with the adaptor toll/interleukin 1 receptor homology domain–containing adaptor molecule 1 (TICAM-1; TRIF). TICAM-1 signals culminate in interferon (IFN) regulatory factor (IRF) 3 activation. Co-culture of mDC pretreated with the TLR3 ligand polyI:C and natural killer (NK) cells resulted in NK cell activation. This activation was triggered by cell-to-cell contact but not cytokines. Using expression profiling and gain/loss-of-function analyses of mDC genes, we tried to identify a TICAM-1–inducing membrane protein that participates in mDC-mediated NK activation. Of the nine candidates screened, one contained a tetraspanin-like sequence and satisfied the screening criteria. The protein, referred to as IRF-3–dependent NK-activating molecule (INAM), functioned in both the mDC and NK cell to facilitate NK activation. In the mDC, TICAM-1, IFN promoter stimulator 1, and IRF-3, but not IRF-7, were required for mDC-mediated NK activation. INAM was minimally expressed on NK cells, was up-regulated in response to polyI:C, and contributed to mDC–NK reciprocal activation via its cytoplasmic tail, which was crucial for the activation signal in NK cells. Adoptive transfer of INAM-expressing mDCs into mice implanted with NK-sensitive tumors caused NK-mediated tumor regression. We identify a new pathway for mDC–NK contact-mediated NK activation that is governed by a TLR signal-derived membrane molecule.

CORRESPONDENCE
Tsukasa Seya:
seya-tu@pop.med.hokudai.ac.jp

Abbreviations used: BMDC, BM-derived DC; IKK, IκB kinase; INAM, IRF-3–dependent NK-activating molecule; IPS-1, IFN promoter stimulator 1; IRF, IFN regulatory factor; mDC, myeloid DC; PRR, pattern recognition receptor; Rae-1, retinoic acid–inducible gene 1; TICAM-1, toll/IL-1 receptor homology domain–containing adaptor molecule 1; TLR, Toll-like receptor.

Natural killer (NK) cells contribute to innate immune responses by killing virus-infected or malignantly transformed cells and by producing cytokines such as IFN-γ and TNF. NK cell activation is determined by a balance of signals from inhibitory and activating receptors. Because ligands of inhibitory receptors include MHC class I and class I–like molecules, the absence of self-MHC expression leads to NK activation (Cerwenka and Lanier, 2001). Approximately 20 receptors contribute to NK activation (Cerwenka and Lanier, 2001; Vivier et al., 2008). When ligands for activating receptors are sufficiently abundant, activating signals overcome inhibitory signals.

There are two currently accepted models for in vivo NK activation. One is that NK cells usually circulate in a naive state and are activated through interaction directly with ligands for pattern recognition receptors (PRRs) expressed by NK cells or interaction with cells that express PRR ligands (Hornung et al., 2002; Sivori et al., 2004). When pathogens enter the host, innate immune sensors, such as Toll-like receptors (TLRs), RIG-I-like receptors,

T. Ebihara and M. Azuma contributed equally to this paper.
T. Ebihara's present address is Howard Hughes Medical Institute, Washington University School of Medicine, St. Louis, MO 63110.

The Rockefeller University Press $30.00
J. Exp. Med. Vol. 207 No. 12 2675-2687
www.jem.org/cgi/doi/10.1084/jem.20091573

Supplemental Material can be found at:
http://jem.rupress.org/content/suppl/2010/11/04/jem.20091573.DC1.html

Published November 8, 2010

JEM

NOD-like receptors, and lectin family proteins, which are PRRs, recognize a variety of microbial patterns (pathogen-associated molecular patterns [PAMPs]; Medzhitov and Janeway, 1997). Mouse NK cells express almost all TLRs (TLR1–3, 4, and 6–9), and some of these are directly activated by pathogens with the help of IL-12, IL-18, IFN-γ, and other cytokines (Newman and Riley, 2007). The other is that naive NK cells tend to be recruited to the draining LNs, where they are primed to be effectors with the help of mature myeloid DCs (mDC) and released into peripheral tissues (Fernandez et al., 1999). In this case, mDCs provide direct activating signals to NK cells through cell–cell contact (Gerosa et al., 2002; Akazawa et al., 2007a; Lucas et al., 2007). mDCs also produce proinflammatory cytokines and IFN-α after recognizing PAMPs (Newman and Riley, 2007). In this mDC-mediated NK activation, however, the molecules and mechanisms in mDC that are dedicated to NK activation in vivo remain to be understood.

In this study, we focused on the molecules that are induced in mDC during maturation by exposure to double-stranded (ds) RNA and the molecules involved in priming NK cells for target killing (Akazawa et al., 2007a). dsRNA of viral origin and the synthetic analogue polyI:C induce NK activation in concert with mDC in vivo and in vitro (Seya and Matsumoto, 2009). PolyI:C is recognized by the cytoplasmic proteins RIG-I/MDA5 and the membrane protein TLR3, both of which are expressed in mDC (Matsumoto and Seya, 2008). Although RIG-I and MDA5 in the cytoplasm deliver a signal to the adaptor protein IFN promoter stimulator 1 (IPS-1; also known as MAVS, VISA, and Cardif) on the outer membrane of the mitochondria (Kawai et al., 2005; Meylan et al., 2005; Seth et al., 2005; Xu et al., 2005), TLR3 in the endosomal membrane recruits the adaptor protein toll/IL-1 receptor homology domain–containing adaptor molecule 1 (TICAM-1)/TRIF (Oshiumi et al., 2003a; Yamamoto et al., 2003a). Both adaptor proteins activate TBK1 and/or IκB kinase (IKK) ε, which phosphorylate IFN regulatory factor (IRF) 3 and IRF-7 to induce type I IFN (Sasai et al., 2006). We previously showed that the TLR3–TICAM-1 pathway in mDC participates in inducing anti-tumor NK cytotoxicity by polyI:C (Akazawa et al., 2007a). mDC matured with polyI:C can enhance NK cytotoxicity through mDC-NK cell–cell contact (Akazawa et al., 2007a). Therefore, we hypothesized that an unidentified protein is up-regulated on the cell surface of mDC through activation of the TLR3–TICAM-1 pathway, and this protein enables mDC to interact with and activate NK cells. This is the first study identifying an IRF-3–dependent NK-activating molecule, which we abbreviated INAM. INAM is a TICAM-1–inducible molecule on the cell surface of BM-derived DCs (BMDCs) that activates NK cells via cell–cell contact. Our data imply that mDCs harbor a pathway for driving NK activation that acts in conjunction with dsRNA and TLR3.

RESULTS

TICAM-1/IRF-3 signal in BMDCs augments NK activation

An in vitro system for evaluating NK activation through BMDC-NK contact was established for this study (Fig. 1 A). A mouse melanoma cell subline B16D8, which was established in our laboratory as a low H-2 expressor (Mukai et al., 1999), was used as an NK target. PolyI:C, WT BMDC, and NK cells were all found to be essential for NK-mediated B16D8 cytolysis in the in vitro assay (Fig. 1 A). PolyI:C-mediated NK activation was at baseline levels in a transwell with a 0.4-μm pore, suggesting the importance of direct BMDC-NK contact for this cytolysis induction (Fig. 1 A). When WT BMDCs were replaced with TICAM-1$^{-/-}$ BMDCs in this system, polyI:C-mediated NK activation was partly abolished (Fig. 1 B; and Fig. S1, A and B). TICAM-1 of BMDC was involved in driving NK activation, and ultimately B16D8 cells were damaged by BMDC-derived NK cells (Fig. 1 B). PolyI:C-mediated NK activation occurred even when WT NK cells were replaced with TICAM-1$^{-/-}$ NK cells (Fig. 1 B), which means that NK activation barely depends on the TICAM-1 pathway in NK cells.

PolyI:C-activated splenic NK cells were i.p. injected into B6 mice to kill B16D8 cells ex vivo, which is consistent with previous studies (McCartney et al., 2009; Miyake et al., 2009), and this polyI:C-mediated NK activation was markedly reduced in IPS-1$^{-/-}$ mice established in our laboratory (Fig. S1 C), suggesting that NK cell activation is induced via not only the TICAM-1 pathway but also the IPS-1 pathway, which was largely comparable with previous studies (McCartney et al., 2009; Miyake et al., 2009). IPS-1 in BMDC was more involved in polyI:C-driven NK cytotoxicity than TICAM-1 but almost equally contributed to NK-dependent IFN-γ induction to TICAM-1 in our setting (Fig. S1 B). In addition, the serum level of IL-12p40 in polyI:C-treated mice was largely dependent on TICAM-1 (Fig. S1 D; Kato et al., 2006; Akazawa et al., 2007a). In the supernatant of polyI:C-stimulated BMDC and the serum samples from polyI:C-treated mice, IL-12p70 was not detected by ELISA (unpublished data). These results suggest that polyI:C activates NK cells largely secondary to mDC maturation, which is sustained by the IPS-1 or TICAM-1 pathway of mDC. Even though NK cells express TLR3, they are only minimally activated by polyI:C alone. Signaling by TICAM-1 in BMDC can augment NK cytotoxicity and IFN-γ production via BMDC/NK contact.

The TICAM-1 pathway activates the transcription factor IRF-3. More precisely, exogenous addition of polyI:C can activate endosomal TLR3 and cytoplasmic RIG-I/MDA5. RIG-I/MDA5 assembles the adaptor IPS-1, which in turn recruits the NAP1–IKK-ε–TBK1 kinase complex and activates both IRF-3 and IRF-7 (Fitzgerald et al., 2003; Yoneyama et al., 2004). For this reason, we examined the role of IRF-3 and IRF-7 in BMDC for activation of NK cells by polyI:C. Activation of IRF-3, but not IRF-7, was required for BMDC to induce NK cytotoxicity (Fig. 1 C). IL-2 (Zanoni et al., 2005), IFN-α (Gerosa et al., 2002), and trans-presenting IL-15 (Lucas et al., 2007) induced by BMDC are reported to be key cytokines for BMDC-mediated NK activation in response to polyI:C. However, even with normal levels of IFN-α production and IL-15 expression (Fig. 1, D and E), TICAM-1$^{-/-}$ BMDCs failed to induce full NK cytotoxicity (Fig. 1 B). In contrast, IRF-7$^{-/-}$ BMDCs, which have impaired IFN-α and IL-15

Published November 8, 2010

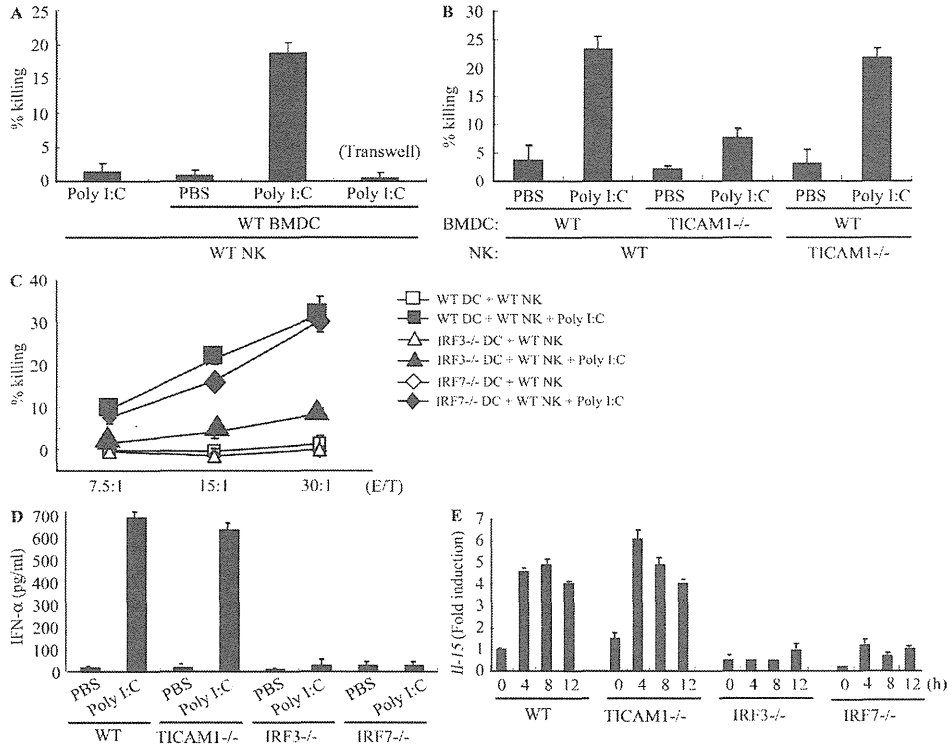

Figure 1. IRF-3 in BMDC controls the capacity to activate NK cells in response to polyI:C. (A and B) WT or TICAM-1$^{-/-}$ NK cells were co-cultured with WT or TICAM-1$^{-/-}$ BMDC in the presence of 10 µg/ml polyI:C for 24 h. NK cytotoxicity against B16D8 was determined by standard ^{51}Cr release assay. E/T = 30. (C) WT NK cells were co-cultured with WT (□, ■), IRF-3$^{-/-}$ (△, ▲), or IRF-7$^{-/-}$ (◇, ◆) BMDC in the presence (■, ▲, ◆) or absence (□, △, ◇) of 10 µg/ml polyI:C for 24 h. NK cytotoxicity against B16D8 was determined by standard ^{51}Cr release assay at the indicated E/T ratio. (D) ELISA of IFN-α in cultures of WT, TICAM-1$^{-/-}$, IRF-3$^{-/-}$, and IRF-7$^{-/-}$ BMDC treated with 10 µg/ml polyI:C for 24 h. (E) Quantitative RT-PCR for IL-15 expression in BMDC stimulated with 10 µg/ml polyI:C. All data are means ± SD of duplicate or triplicate samples from one experiment that is representative of three.

expression, fully activated NK cells (Fig. 1, C–E). Hence, in BDMCs, the TICAM-1–IRF-3 pathway, rather than other cytokines, appears to induce cell surface molecules that mediate BMDC/NK contact and evoke NK cytotoxicity.

Identification of INAM

To identify the NK-activating cell surface molecule on BMDC, we performed microarray analysis on polyI:C-stimulated BMDC prepared from TICAM-1$^{-/-}$ and WT mice. The results yielded nine TICAM-1–inducible molecules with transmembrane motifs (Table S1). Six were induced in an IRF-3–dependent manner, whereas three were still induced in IRF-3$^{-/-}$ BMDC. The NK-activating ability of the products of these genes was investigated by introduction of lentivirus expression vector into IRF-3$^{-/-}$ BMDC. BMDCs with the transduced genes were co-cultured with WT NK cells and polyI:C, and the NK-activating ability was evaluated by determining IFN-γ in the 24-h co-culture. NK cells, but not the gene-transduced BMDCs, produced IFN-γ in the presence of polyI:C. Finally, we identified a tetraspanin-like molecule that satisfied our evaluation criteria (IFN-γ and cytotoxicity) on the mDC-NK activation and named this molecule INAM. INAM clearly differed from other tetraspanins like CD9, CD63, CD81, CD82, and CD151 in the predicted structure. Mouse INAM is a 40–55-kD protein with one N-glycosylation site and possesses four transmembrane motifs (Fig. 2, A and B). Western blotting analysis of INAM-transfected cells under nonreducing conditions showed no evidence of multimers (Fig. 2 B). The N-terminal and C-terminal regions of INAM are in the cytoplasm because anti-Flag antibody did not detect C-terminal Flag-tagged INAM until cells were permeabilized (unpublished data).

Alignment of the predicted amino acid sequence of mouse INAM with that of the human orthologue revealed that the two INAMs shared a 71.7% amino acid identity. INAM is also called FAM26F (Table S1) and is in the FAM26 gene family (Bertram et al., 2008; Dreses-Werringloer et al., 2008). Sequence database searches identified six mouse INAM paralogs. Although FAM26A/CALHM3, FAM26B/CALHM2, and FAM26C/CALHM1 are located on chromosome 19, FAM26D, FAM26E, and FAM26F/INAM are on chromosome 10. Only INAM was inducible with TLR agonists (unpublished data). All FAM26 family proteins have three or four transmembrane motifs predicted by the TMHMM Server (version 2.0). Human CALHM1 has a conserved region (Q/R/N site)

Published November 8, 2010

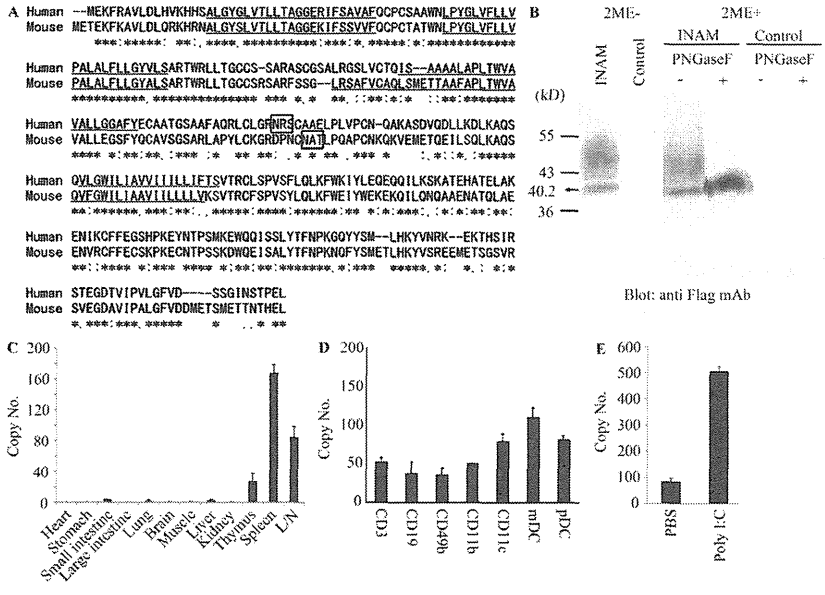

Figure 2. Sequence alignment of INAM and expression of INAM. (A) Sequence alignment of human and mouse INAM. Asterisks, identical residues; double dots, conserved substitutions; single dots, semiconserved substitutions; box, N-glycosylation site; underline, transmembrane motif. (B) Immunoblot analysis of lysates of 293FT cells transfected with plasmid encoding Flag-tagged INAM. PNGase, *N*-glycosidase. 2ME, 2-mercaptoethanol. (C and D) Quantitative RT-PCR for INAM expression in mouse tissue (C) and spleen cells (D). $CD3^+$, $CD19^+$, $DX5^+$, $CD11b^+$, $CD11c^+$, mDC ($CD11c^+PDCA1^-$), and plasmacytoid DC (pDC; $CD11c^+PDCA1^+$) cells were isolated from splenocytes by cell sorting. Data are expressed as copy number per 10^4 copies of HPRT. Data shown are means ± SD of triplicate samples from one experiment that is representative of three. (E) Augmented INAM expression in LN cells after polyI:C stimulation. WT mice were i.p. injected with 100 µg polyI:C or control buffer. After 24 h, inguinal, axillary, and mesenteric LN were harvested and RNA was extracted from the LN cells. The levels of the INAM mRNA were measured by real-time PCR. The results were confirmed in two additional experiments. Data represent mean ± SD.

with ion channel properties at the C-terminal end of the second transmembrane motif that controls cytoplasmic Ca^{2+} levels (Dreses-Werringloer et al., 2008). However, the Q/R/N site was not found in INAM. CALHM1, 2, and 3 are highly expressed in brain. Quantitative RT-PCR revealed that INAM expression was high in spleen and LNs but low in thymus, liver, lung, and small intestine (Fig. 2 C), although expression of the other two FAM26 family members from chromosome 10 was highest in brain (not depicted). All splenocytes examined ($CD3^+$, $CD19^+$, $DX5^+$, $CD11b^+$, $CD11c^+$, mDCs [$CD11c^+$ $PDCA1^-$], and plasmacytoid DCs [$CD11c^-PDCA1^+$]) expressed INAM to some levels (Fig. 2 D). The INAM expression was inducible by polyI:C in LN cells (Fig. 2 E); the induction levels were more prominent in myeloid cells than in lymphocytes in the LNs (Fig. S2 A). $NKp46^+$ and $DX5^+$ NK cells also expressed INAM with low levels and the levels were mildly increased by polyI:C stimulation (Fig. S2 A and not depicted). Notably, only $CD45^+$ cells expressed INAM, which excludes the participation of contaminating stromal cells in the INAM up-regulation (Fig. S2 B).

BMDC INAM activates NK cells

WT and IRF-$7^{-/-}$ BMDCs induced high NK cytotoxicity in response to polyI:C, whereas TICAM-$1^{-/-}$, IPS-$1^{-/-}$, and IRF-$3^{-/-}$ BMDC showed less NK activation (Fig. 1, B and C; and Fig. S1). INAM expression profile by polyI:C stimulation was then examined using WT, IRF-$3^{-/-}$, IRF-$7^{-/-}$, and TICAM-$1^{-/-}$ BMDCs. Stimulation with polyI:C induced INAM at normal levels in IRF-$7^{-/-}$ BMDC but at decreased levels in IRF-$3^{-/-}$ and TICAM-$1^{-/-}$ BMDC (Fig. 3 A). The expression profiles of INAM in polyI:C-stimulated BMDC were in parallel with those inducing NK activation. BMDCs express a variety of TLRs (Iwasaki and Medzhitov, 2004), but other TLR ligands, Pam_3CSK_4 for TLR1/2, Malp2 for TLR2/6, and CpG for TLR9, barely induced INAM on BMDC. High induction of INAM was observed in BMDC stimulated with LPS as well as polyI:C (Fig. 3 B), both of which can activate TICAM-1 to induce IRF-3 and IFN-α activation (Fitzgerald et al., 2003; Oshiumi et al., 2003a,b; Yamamoto et al., 2003a,b). Because INAM is an IFN-inducible gene (Fig. 3 B), INAM induction may be amplified by type I IFNs.

We next examined whether INAM was localized to the cell surface membrane in BMDC. Immunofluorescence analysis showed Flag-tagged INAM on the cell surface of BMDC. Plasma membrane expression of INAM was also confirmed by cell surface biotinylation (Fig. S3). Although the lentivirus inefficiently infected BMDC, GFP expression levels were similar in cells with control virus and those with INAM-expressing virus (Fig. 3 C). Transduction efficiency and expression from the lentivirus vector were adjusted using GFP expression (not depicted), and surface INAM expression was further confirmed with BMDC, NK cells, and INAM-expressing BaF3 (INAM/BaF3) cells, in some cases using polyclonal antibody (Ab) against INAM (Fig. S4).

We then examined whether overexpressing INAM resulted in signaling that directed BMDC maturation and production of cytokines, including IFN-α and IL-12p40, which are reported to enhance NK activity (Gerosa et al., 2002; Sivori et al., 2004; Lucas et al., 2007). The status of INAM-transduced BMDC was assessed by CD86 expression and cytokine production, and no significant differences in these maturation markers were seen in BMDC overexpressing INAM (Fig. S5). In the same setting, no IL-12p70 was

Published November 8, 2010

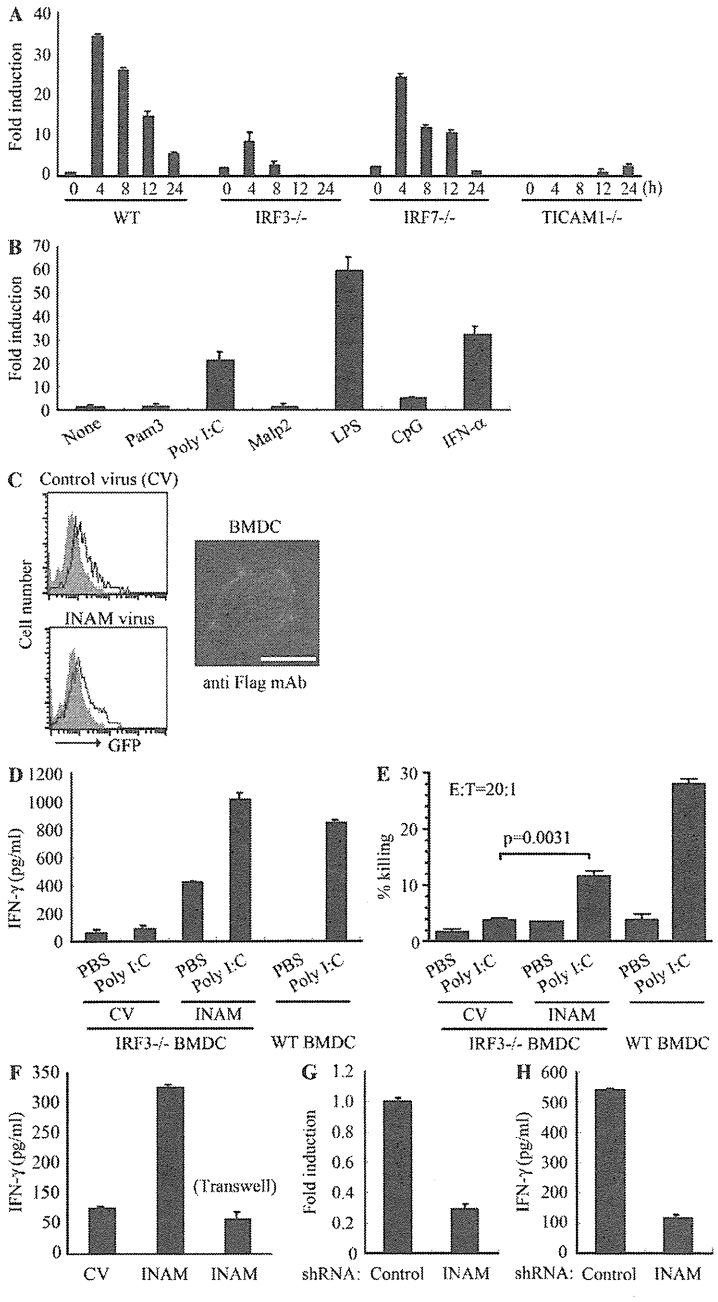

Figure 3. INAM in BMDC participates in DC-mediated NK activation. (A) Quantitative RT-PCR for INAM expression in WT, TICAM-1$^{-/-}$, IRF-3$^{-/-}$, and IRF-7$^{-/-}$ BMDC stimulated with 10 μg/ml polyI:C. (B) Quantitative RT-PCR for INAM expression in WT BMDC stimulated by 100 ng/ml LPS, 10 μg/ml polyI:C, 1 μg/ml Pam3, 100 nM Malp-2, 10 μg/ml CpG, and 2,000 IU/ml IFN-α for 4 h. (C) BMDCs were transduced with Flag-tagged INAM-expressing lentivirus or control lentivirus. GFP expression in the BMDC was determined by flow cytometry, and subcellular localization of INAM was examined by immunofluorescence assay using anti-Flag mAb. Shaded peak, noninfected control; Blank peak, infected BMDC. Bar, 10 μm. (D) ELISA of IFN-γ induced by WT NK cells co-cultured with WT BMDC or IRF-3$^{-/-}$ BMDC transfected with control lentivirus (CV) or INAM-expressing lentivirus (INAM) with/without 10 μg/ml polyI:C. (E) Cytotoxicity against B16D8 by NK cells co-cultured with BMDC transfected with control or INAM-expressing lentivirus with/without 10 μg/ml polyI:C for 24 h. (F) ELISA of IFN-γ induced by WT NK cells co-cultured with IRF-3$^{-/-}$ BMDC transfected with control lentivirus (CV) or INAM-expressing lentivirus (INAM) with 10 μg/ml polyI:C. In some experiments, a transwell was inserted between the INAM-transduced BMDC and NK cells to separate the cells. (G) Quantitative RT-PCR for expression of INAM in BMDC transduced with INAM-shRNA (INAM) or scrambled shRNA (control) and cultured for 48 h. (H) IFN-γ production by WT NK cells determined using ELISA after coculturing with control or the shRNA transfected-BMDC (INAM) and 10 μg/ml polyI:C for 24 h. All data shown are means ± SD of triplicate samples from one experiment that is representative of three.

detected by ELISA (unpublished data). In addition, polyI:C-mediated NK activation occurred in BMDC expressing an INAM mutant lacking the cytoplasmic C-terminal region (193–327 aa; Fig. 4, A and B), excluding the participation of the cytoplasmic region in BMDC maturation signaling.

To investigate whether INAM could reconstitute NK-activating ability in IRF-3$^{-/-}$ BMDC, we transduced INAM into IRF-3$^{-/-}$ BMDC and incubated BMDC with NK cells. Overexpression of INAM in IRF-3$^{-/-}$ BMDC induced NK IFN-γ production and NK cytotoxicity against B16D8, and this NK activation was further enhanced by the addition of polyI:C (Fig. 3, D and E). Thus, polyI:C may also work for NK activation. Direct cell–cell contact with NK cells was required for INAM in IRF-3$^{-/-}$ BMDC to function on enhancing NK activity (Fig. 3 F).

We further confirmed this issue using WT BMDC by shRNA gene silencing. We silenced the INAM gene in BMDC using the lentiviral vector pLenti-dest-IRES-hrGFP and monitored expression by GFP. Because transfection efficiency was relatively high in this case compared with that shown in Fig. 3 C, the expression level of INAM had decreased by ~75% in WT BMDC compared with the nonsilenced control (Fig. 3 G and Fig. S6 A). Although the level of the endogenous INAM protein was not very high, we confirmed that INAM protein was also decreased by shRNA with immunoblotting using anti-INAM pAb (Fig. S7 A). PolyI:C response of BMDC-inducible cytokines tested was not altered by INAM silencing in BMDC (Fig. S6 B). Yet this INAM RNA interference caused a significant decrease in NK cell IFN-γ production after co-culture of the INAM knockdown BMDCs and WT NK cells with polyI:C (Fig. 3 H). Collectively, these results indicate that INAM is downstream of IRF-3 in BMDC and is involved in the activation of NK cells by BMDC.

Published November 8, 2010

Using an INAM-expressing stable BaF3 cell line (INAM/BaF3), we tested the possibility that INAM is an activating ligand for NK cells. As a positive control, we produced a stable BaF3 cell line expressing Rae-1α (Fig. 5 A) which is a ligand for the NK-activating receptor NKG2D (Cerwenka et al., 2000). Although Rae-1α/BaF3 cells were easily damaged by IL-2–activated NK cells, INAM/BaF3 cells were not (Fig. 5 B). In this context, addition of IRF-3$^{-/-}$ BMDC to this culture with BaF3 and NK cells led to slight augmentation of IFN-γ induction irrespective of the presence of INAM on BaF3 cells (Fig. 5 C), and β2-microglobulin$^{-/-}$ BMDC barely affected the IFN-γ level (not depicted). These results suggest that an INAM-containing molecular matrix, rather than INAM alone, acts toward NK cells. Alternatively, INAM may selectively function with specific mDC molecules to activate NK cells.

INAM on NK cells is required for efficient NK activation

mDCs were previously shown to be required for efficient NK activation in vivo and in vitro (Akazawa et al., 2007a). We found that INAM was minimally present in BMDCs and NK cells and that polyI:C acts on both (Figs. S2 A; and Fig 3, D and E). Tetraspanin-like molecules tend to work as scaffolds for heteromolecular complexes that contain molecules functioning in a cis- or trans-adhesion manner to exert intercellular or extracellular functions. Thus, the function of INAM may not be confined to mDC, so we studied the function of INAM on NK cells. In NK cells, INAM was also inducible by polyI:C (Fig. 6 A and Fig. S2 A), and the induction of INAM was abrogated completely in IRF-3$^{-/-}$ NK cells and moderately in TICAM1$^{-/-}$ NK cells (Fig. 6 B). This suggests that polyI:C also acts on NK cells and induces INAM through IPS-1/IRF-3 activation when NK cells are co-cultured with BMDC and polyI:C.

To investigate whether INAM induced in NK cells is associated with BMDC-mediated NK activation, we performed the following experiments (Fig. 6 C). INAM-transduced IRF-3$^{-/-}$ BMDCs were incubated with polyI:C for 4 h, and then the aliquot was mixed with WT NK cells in the presence of polyI:C (Fig. 6 C, left two lanes). A moderate increase of IFN-γ was observed as in Fig. 3 D. In the remainder,

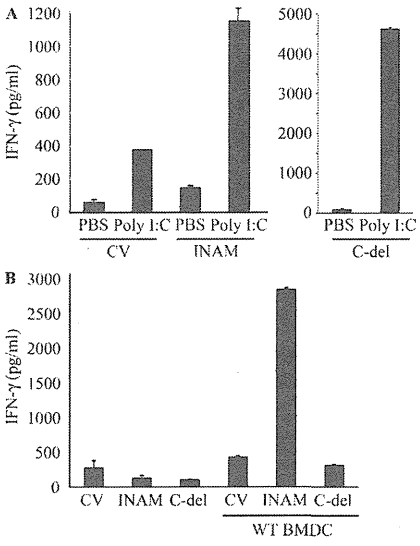

Figure 4. Role of the cytoplasmic tail of INAM. (A) The C-terminal region of INAM was not required for BMDC-mediated NK activation. ELISA of IFN-γ by WT NK cells co-cultured with IRF-3$^{-/-}$ BMDCs transfected with control lentivirus (CV) or a lentivirus expressing intact INAM or a mutant INAM lacking the C-terminus (C-del INAM) with/without 10 μg/ml polyI:C. Data shown are means ± SD of triplicate samples from one experiment representative of three. (B) The cytoplasmic tail of INAM is indispensable for NK IFN-γ induction. INAM or C-del INAM (A) was expressed on IRF-3$^{-/-}$ NK cells. The INAM (or C-del INAM)-expressing IRF-3$^{-/-}$ NK cells were incubated with or without WT BMDC for 24 h. IFN-γ levels in the supernatants were determined by ELISA. One representative result out of several similar experiments is shown. Data represent mean ± SD.

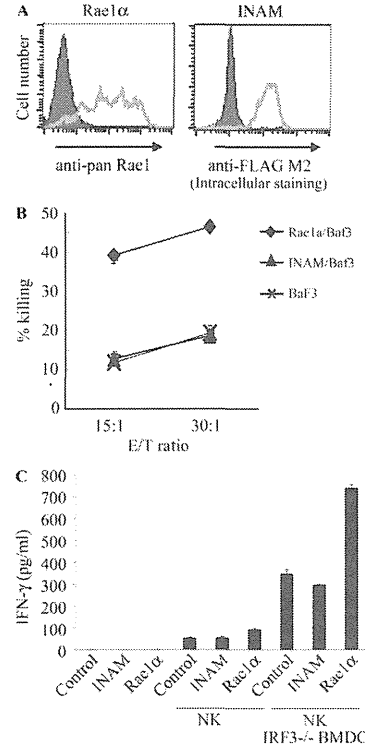

Figure 5. INAM is not an NK-activating ligand. (A) Flow cytometry for Rae-1 and Flag-tagged INAM in stable BaF3 lines. Shaded peak, untransfected control BaF3 staining with anti-pan-Rae-1 Ab or anti-Flag M2 antibody; open peak, stable Rae-1α/BaF3 or stable Flag-tagged INAM/BaF3 staining with anti-pan-Rae-1 antibody or anti-Flag M2 antibody. (B) Cytotoxicity against control BaF3, Rae-1α/BaF3, and INAM/BaF3 by NK cells treated with 1,000 IU/ml IL-2 for 3 d. Data shown are means ± SD of triplicate samples from one experiment representative of three. (C) NK activation is augmented by coexistent BMDC irrespective of INAM expression. NK cells were cultured with 1,000 IU/ml IL-2 for 3 d. 2 × 10^5 NK cells, 10^5 BaF3 cells, and 10^5 IRF-3$^{-/-}$ BMDCs were co-cultured in 200 μl/well and IFN-γ in the supernatants were measured by ELISA. Data show one of two similar experimental results. Data represent mean ± SD.

Published November 8, 2010

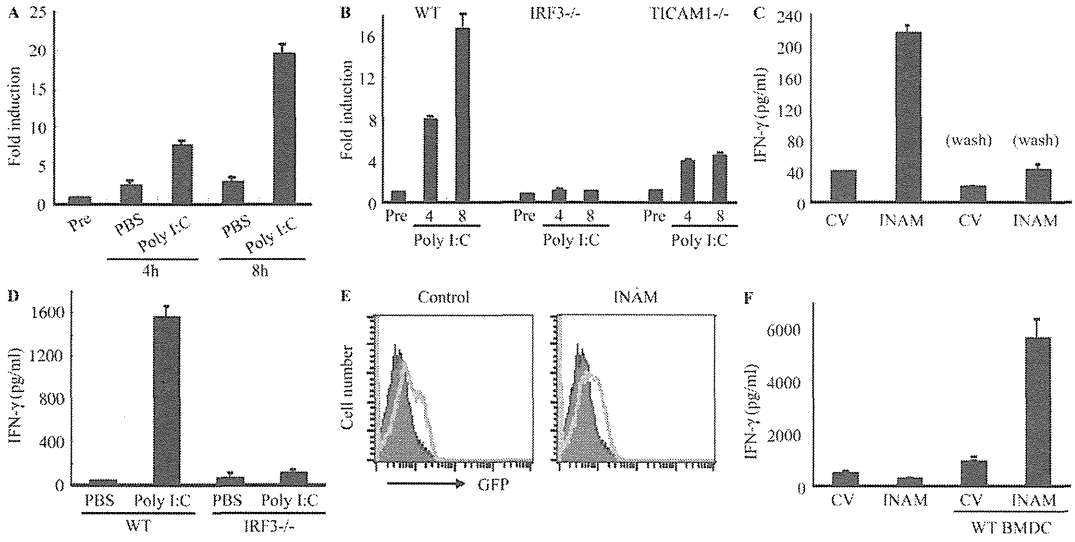

Figure 6. INAM on NK cells contributes to efficient NK activation mediated by mDC. (A and B) Quantitative RT-PCR for INAM expression in WT, TICAM1$^{-/-}$, or IRF-3$^{-/-}$ NK cells stimulated with 50 µg/ml polyI:C. Data shown are means of duplicate or triplicate samples from one experiment that is representative of three. (C) IRF-3$^{-/-}$ BMDCs were transfected with control lentivirus (CV) or INAM-expressing lentivirus (INAM) before treatment with 10 µg/ml polyI:C for 4 h. BMDCs in some wells were washed to remove polyI:C before WT NK cells were added (Wash). IFN-γ production by NK cells was determined by ELISA after 24 h of culture. Data show one of two similar experimental results. (D) ELISA of IFN-γ in co-culture of WT or IRF-3$^{-/-}$ NK cells and WT BMDC with/without 10 µg/ml polyI:C. (E and F) NK cells were transfected with control lentivirus or INAM-expressing lentivirus and cultured with 500 IU/ml IL-2 for 3 d. After determining transfection efficiency by GFP intensity using flow cytometry, cells were cultured with/without BMDC for 24 h and IFN-γ production in the supernatant determined by ELISA. Shaded peak, noninfected control; open peak, infected BMDC. All data are means ± SD of triplicate samples from one experiment that is representative of three.

we washed polyI:C out and cultured the cells with WT NK cells (Fig. 6 C, right two lanes). Under these conditions, in which polyI:C acted not on NK cells but only on BMDC, little NK activation was observed (Fig. 6 C). Furthermore, IRF-3$^{-/-}$ NK cells produced little IFN-γ when co-cultured with WT BMDC and polyI:C (Fig. 6 D). INAM-overexpressing IRF-3$^{-/-}$ BMDC required IRF-3 in NK cells for efficient BMDC-mediated production of IFN-γ from NK cells (Fig. 6 D). We next transduced INAM into IRF-3$^{-/-}$ NK cells using a lentivirus (INAM/pLenti-IRES-hrGFP) to reconstitute NK IFN-γ–producing activity. After many trials with various setting conditions, we found that ~15% of the DX5^{+} NK cell population was both GFP-positive and stained with anti-FLAG mAb when treated with high doses of INAM-expressing lentivirus vector (Fig. S7 B). When IRF-3$^{-/-}$ NK cells were infected with smaller amounts of INAM-expressing lentiviral vector and cultured for 3 d with high concentrations of IL-2 (500 IU/ml), slight but significant GFP expression was confirmed by FACS (Fig. 6 E). Then, the INAM-transduced IRF-3$^{-/-}$ NK cells were co-cultured with WT BMDC. The IRF-3$^{-/-}$ NK cells with INAM expression secreted IFN-γ at significantly higher levels than controls in the presence of WT BMDC (Fig. 6 F). These data indicate that INAM is induced by polyI:C through IRF-3 activation, not only in BMDCs but also in NK cells, and that INAM on NK cells synergistically works with INAM on BMDC for efficient NK cell activation. Both INAMs on BMDC and NK cells are essential for BMDC-mediated NK activation.

We next checked the function of the C-terminal stretch of INAM in NK activation. Although intact INAM works in NK cells to produce IFN-γ in response to BMDC (Fig. 6 F), introduction of C-del INAM into IRF-3$^{-/-}$ NK cells did not result in high induction of IFN-γ in response to BMDC (Fig. 4 C). Thus, INAM participates in NK activation through its cytoplasmic regions, which has no significant role in BMDC for NK activation.

Anti-tumor NK activation via INAM-expressing BMDCs in vivo

mDC-mediated NK activation induces anti-tumor NK cells, which cause regression of NK-sensitive tumors (Kalinski et al., 2005; Akazawa et al., 2007a). We tested the in vivo function of INAM-expressing BMDC using B16D8 tumor-bearing mice. BMDCs were used 24 h after transfection with either INAM/pLenti-IRES-hrGFP or control pLenti-IRES-hrGFP and injected twice a week s.c. around a preexisting tumor in tumor-implanted mice, beginning 11–13 d after tumor challenge. INAM-expressing BMDC significantly retarded tumor growth (Fig. 7 A). Tumor retardation was abrogated by depletion of NK1.1-positive cells (Fig. 7 B). Thus, INAM expression on BMDC contributed to anti-tumor NK activation in vivo.

When the control or INAM-expressing IRF-3$^{-/-}$ BMDCs were co-cultured with WT NK cells in vitro, there was no induction of the mRNA of TRAIL and granzyme B in

Published November 8, 2010

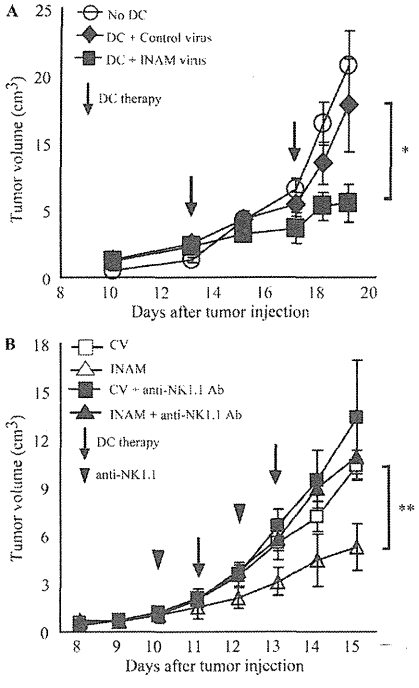

Figure 7. INAM on BMDC retarded B16D8 tumor growth in an NK-dependent manner. (A) Tumor volume after DC therapy using BMDC expressing INAM. B16D8 cells were s.c. injected into C57BL/6 mice and, 11–13 d later, medium only (○) or BMDC (10^6/mouse) transfected with control lentivirus (◆) or those with INAM-expressing lentivirus (■) were administered s.c. near the tumor at the time indicated by the open arrow. *, P = 0.043. Data represent mean ± SD. (B) Abrogation of INAM-dependent tumor regression by administration of NK1.1 Ab. For depletion of NK cells, antiNK1.1 mAb was injected i.p. 1 d before treatment of BMDC (arrowheads). Tumor volume in every mouse group was sequentially monitored. Data represent mean ± SD (n = 3) and are representative of two experiments. Statistical analyses were made with the Student's t test. **, P = 0.017.

NK cells (Fig. 8 A). TRAIL and granzyme B were induced in NK cells by the addition of polyI:C to the mixture, and INAM expression in BMDC up-regulated mRNA levels of TRAIL and granzyme B (Fig. 8 A). In vivo administration studies were performed with polyI:C-treated WT BMDC or INAM-expressing IRF-$3^{-/-}$ BMDC to test their ability to up-regulate the mRNA levels of TRAIL and granzyme B in NK cells in draining LN (Fig. 8 B). INAM-expressing IRF-$3^{-/-}$ BMDC showed comparable abilities to up-regulate the killing effectors with polyI:C-treated BMDC (Fig. 8 B). Collectively, INAM has therapeutic potential for NK-sensitive tumors by activating NK cells.

DISCUSSION

Previous studies demonstrated that mDC–NK interaction leads to direct NK activation and damages NK target cells in vitro (Gerosa et al., 2002; Sivori et al., 2004; Akazawa et al., 2007a; Lucas et al., 2007). In addition, mDCs initiate NK cell–mediated innate anti-tumor immune responses in vivo (Kalinski et al., 2005; Akazawa et al., 2007a,b). Systemic administration of polyI:C unequivocally results in activation of peripheral NK cells (Lee et al., 1990; Sivori et al., 2004; Akazawa et al., 2007a). Although the molecular mechanism by which mDCs prime NK cells was still unclear, the TICAM-1 pathway and IPS-1 pathway have been reported to participate in polyI:C-mediated mDC maturation that drives NK activation (Akazawa et al., 2007a; McCartney et al., 2009; Miyake et al., 2009). We have shown in an earlier study that mDCs disrupted in the TLR3–TICAM-1 pathway abrogate NK cell activation (Akazawa et al., 2007a,b). In TICAM-$1^{-/-}$ mice, NK-sensitive implant tumors grew as well as those in WT mice depleted of NK cells (Akazawa et al., 2007a). mDCs gain high anti-tumor potential against B16D8 implant tumors through lentiviral transfer of TICAM-1, which is attributable to NK activation (Akazawa et al., 2007a). We further showed that TICAM-1 is a critical molecule for mDC to induce NK cell IFN-γ, as well as IPS-1, and participates in driving NK cytotoxicity to a lesser extent than IPS-1. In this paper, we clarified a molecular mechanism by which mDCs immediately promote NK cell functions in vitro and in vivo.

Our findings showed that IRF-3 is the transcription factor that is downstream of TICAM-1 responsible for maturing mDC to an NK-activating phenotype. We discovered that INAM, a membrane-associated protein, is up-regulated on the surface of mDC by polyI:C stimulation and activates NK cells via cell–cell contact. Furthermore, we found that NK cells also express INAM on their cell surface after polyI:C stimulation. mDC–NK activation by polyI:C can be reproduced with INAM-transduced mDC and NK cells, and adoptive transfer experiments show that INAM-overexpressing mDC may have therapeutic potential against MHC-low melanoma cells in an NK-dependent manner. These functional properties of INAM-expressing mDC fit the model of mDC priming NK activation. Ultimately, INAM appears to be the key molecule in the previously reported mechanism of mDC–NK contact activation.

After the submission of this manuscript, two papers were published that found that the MDA5–IPS-1 pathway in mDC is more important for driving NK activation, particularly in vivo (McCartney et al., 2009; Miyake et al., 2009). Our data also support this point using the IPS-$1^{-/-}$ mice we established (Fig. S1). However, polyI:C, when i.v. administered into mice, may stimulate other systemic cells in addition to $CD8^+$ mDC in vivo (McCartney et al., 2009). The difference among the two (McCartney et al., 2009; Miyake et al., 2009) and this study may be attributed to the setting conditions, which are not always comparable. Moreover, it remains to be settled whether TICAM-1 and IPS-1 take the same INAM complex as a common NK activator in mature mDC and whether TLR3 (or MDA5) KO is equivalent to TICAM-1 (or IPS-1) KO in the mDC–NK activation model. In either case, however, up-regulation of mDC TICAM-1–mediated NK cytotoxicity and IFN-γ induction are feasible with polyI:C under three different conditions (Akazawa et al., 2007a; McCartney et al., 2009; Miyake et al., 2009). Our results infer that INAM participates in at least these mDC–NK interactions.

Published November 8, 2010

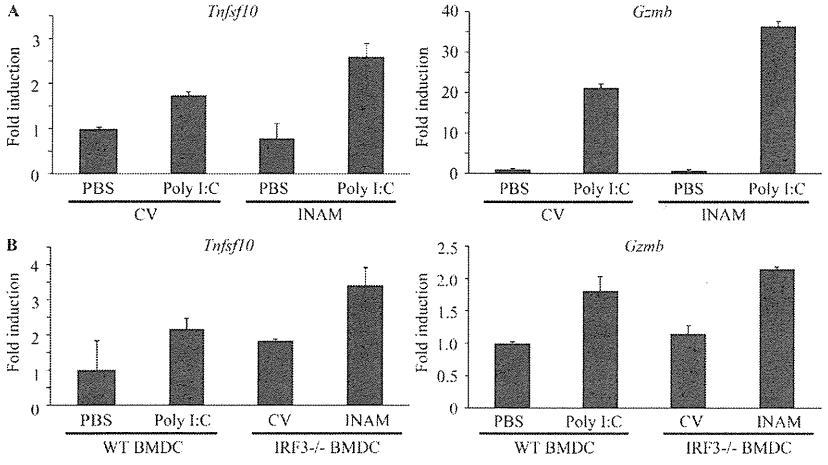

Figure 8. INAM-mediated induction of TRAIL and granzyme B in BMDC. (A) In vitro induction of TRAIL (Tnfsf10) and granzyme B (Gzmb) mRNA by INAM-expressing BMDC. BMDCs (IRF-3$^{-/-}$) were infected with INAM-expressing virus or CV as in Fig. S4. After 24 h, the BMDCs (IRF-3$^{-/-}$) were incubated with WT NK cells at DC/NK = 1:2. 8 h later, DX5^{+} cells were collected by FACS sorting and their RNA was extracted to determine the mRNA levels of the indicated genes. A representative result of three similar experiments are shown. (B) In vivo induction of TRAIL and granzyme B mRNA by INAM-expressing BMDC. WT BMDCs were stimulated with 10 µg/ml polyI:C or medium only. IRF-3$^{-/-}$ BMDCs were infected with CV or INAM-expressing vector. These BMDCs were allowed to stand for 24 h and then 5×10^5 cells were injected into footpads of WT mice. After 48 h, DX5^{+} cells were collected from the inguinal LN by FACS sorting. RNA of the cells was extracted and the levels of the indicated mRNA were determined by real time PCR. Data show one of two experiments with similar results. Data in A and B represent mean ± SD.

PolyI:C activates IRF-3 through the two pathways involving the adaptors IPS-1 and TICAM-1 (Yoneyama et al., 2004; Kato et al., 2006; Matsumoto and Seya, 2008). The two pathways share the complex of IRF-3–activating kinase, NAP1, IKK-ε, and TBK1 that is downstream of adaptors (Sasai et al., 2006). Nevertheless, these pathways are capable of inducing several genes unique to each adaptor. Although IFN-α production by in vivo administration of polyI:C is largely dependent on the IPS-1 pathway, IL-12p40 is mainly produced by the TICAM-1 pathway (Kato et al., 2006). Therefore, it is not surprising that INAM induction is predominant in the TICAM-1 pathway in polyI:C-stimulated BMDC (Fig. 3 A). What happens in IRF-7$^{-/-}$ BMDCs in terms of INAM induction and what mechanism sustains BMDC IPS-1–mediated or MyD88-mediated activation of NK cells (Azuma et al., 2010) will be issues to be elucidated in the future.

Although IRF-3–regulated cell surface INAMs are required for efficient interaction between BMDC and NK cells, the mechanism by which forced expression of INAM causes signaling for BMDC maturation is still unknown. Although the NK-activating capacity of BMDCs is usually linked to their maturation, neither cytokines in NK activation, including IFN-α and IL-12p70, nor costimulators, such as CD40 and CD86, were specifically induced in mDC by INAM expression (Fig. S5). INAM has a C-terminal cytoplasmic stretch (Fig. 4 A), and we tested the function of this region by a deletion mutant (C-del INAM). This region in BMDC barely participates in driving NK activation because no decrease of IFN-γ induction by NK cells was observed with IRF-3$^{-/-}$ BMDC supplemented with C-del INAM compared with control INAM. Thus far, no significant signal alteration has been detected in BMDC supplemented with INAM by lentivirus.

In contrast, INAM-transduced IRF-3$^{-/-}$ NK cells produced IFN-γ in concert with BMDCs like WT NK cells (Fig. 6 F). So far we have no evidence suggesting that this kind of INAM overexpression is actually occurring in vivo. However, introduction of C-del INAM into IRF-3$^{-/-}$ NK cells did not result in high induction of IFN-γ in response to BMDC (Fig. 4 C). Together with the data on INAM expression in BMDC, this infers that the INAM cytoplasmic region signals for NK activation in NK cells. The one-way role of the cytoplasmic tail in NK activation will be an issue for further analysis.

In this study, IL-15 was found to be up-regulated by polyI:C in BMDC. The remaining NK activity in the resting population of NK cells co-cultured with TICAM-1$^{-/-}$ BMDC and polyI:C (Fig. 1 B) suggests that IL-15 has some effect in our system, and other studies suggest this as well (Ohteki et al., 2006; Brilot et al., 2007; Lucas et al., 2007; Huntington et al., 2009). However, we did not observe decreased IL-15 expression in the TICAM-1$^{-/-}$ BMDC that could not activate NK cells (Fig. 1 E). Several molecules, such as B7-H6/NKp30 (Brandt et al., 2009), CD48/2B4 (Kubin et al., 1999), and NKG2D ligands/NKG2D (Cerwenka et al., 2000), have been identified as ligand/receptor molecules in mDC–NK reciprocal activation by in vitro co-culture. In in vitro co-culture systems (Fig. S1), the IPS-1 pathway in BMDC has a pivotal role in not only type I IFN but also IL-15 induction. INAM identified in this paper serves a unique function in the in vivo induction of NK activation and may offer a tool to investigate the reported mDC-mediated NK activation.

Rae-1 was reported as a molecule with MHC-like structure (Zou et al., 1996) and later identified as a mouse NKG2D ligand (Cerwenka et al., 2000). Although Rae-1 is a GPI-anchored protein with no cytoplasmic sequences (Nomura et al., 1996), it can act as an NK-activating ligand (Cerwenka et al., 2000, 2001; Masuda et al., 2002). Mouse BaF3 cells become NK-sensitive after forced expression of Rae-1α (Masuda et al., 2002). Actually, mouse macrophages induce Rae-1 expression in response to TLR stimuli (Hamerman et al., 2004). In contrast,

Published November 8, 2010

JEM

INAM-expressing stable BaF3 cell lines (INAM/BaF3) did not reveal a function as an NK cell–activating ligand. NK cell cytotoxicity is directed against Rae-1α/BaF3 cells but not against INAM/BaF3 cells (Fig. 5). Therefore, INAM does not represent a typical NK cell–activating ligand. For NK activation, INAM on BMDC appears to require other molecules that are expressed in BMDC but not in BaF3.

INAM has four transmembrane regions, similar to the cell adhesion tetraspanins, which may support cell–cell contact (Levy and Shoham, 2005). Tetraspanins provide a scaffold that facilitates complex formation with associated proteins. INAM on BMDC and NK cells may use cell–cell interaction to assemble in a synaptic formation to activate NK cells. Because the protein constituents of the tetraspanin complexes are cell specific, we are interested in finding partners for INAM that might participate in efficient BMDC–NK interaction. TLR-inducible cell–cell contact may occur through INAM in an immune cell–specific manner. Gene disruption of this INAM will facilitate clarifying this issue. The identification of INAM defines a novel pathway in mDC–NK reciprocal interaction. This study will lead to further research on the molecules that form complexes on BMDC and NK cells to facilitate BMDC–NK interaction.

MATERIALS AND METHODS

Mice. All mice were backcrossed with C57BL/6 mice more then seven times before use. TICAM-1$^{-/-}$ (Akazawa et al., 2007a) and IPS-1$^{-/-}$ mice were generated in our laboratory. IRF-3$^{-/-}$ (Sato et al., 2000) and IRF-7$^{-/-}$ mice (Honda et al., 2005) were provided by T. Taniguchi (University of Tokyo, Tokyo, Japan). All mice were maintained under specific pathogen-free conditions in the animal facility of the Hokkaido University Graduate School of Medicine. Animal experiments protocols and guidelines were approved by the Animal Safety Center, Hokkaido University, Japan.

Cells. The B16D8 cell line was established in our laboratory as a subline of B16 melanoma (Tanaka et al., 1988). This subline was characterized by its low or virtually no metastatic properties when injected s.c. into syngeneic C57BL/6 mice. B16D8 was cultured in RPMI 1640/10% FCS. The mouse B cell line BaF3 was obtained from American Type Culture Collection and cultured in RPMI 1640/10% FCS/2 μM 2ME/5 ng/ml IL-3. Mouse NK cells (DX5$^+$ cell) were positively isolated with MACS Beads (Miltenyi Biotec). Mouse BMDCs were prepared as previously reported (Akazawa et al., 2007a).

For purification of cells from spleen or LN, these tissues were treated with 400 IU MandleU/ml collagenase D (Roche) at 37°C for 25 min in HBSS (Sigma-Aldrich). Then EDTA was added, and the cell suspension was incubated for an additional 5 min at 37°C. After removal of RBC with ACK lysis buffer, splenocytes and LN cells were stained with CD45-FITC, CD3ε-PE, CD19-PE, DX5-PE, CD11b-FITC (eBioscience), and CD11c-FITC (BioLegend) and sorted by a FACSAria II (BD). The purity of sorted cells were >96%.

Construction and expression. Mouse INAM cDNA (A630077B13Rik) was obtained from RIKEN and placed into expression vector pEFBOS and pLenti-IRES-hrGFP, both of which provide the specialized components needed for expression of a recombinant C-terminal FLAG fusion (Akazawa et al., 2007a). For construction of shRNA-expressing lentivirus vector, The ClaI–XhoI fragment of pLenti6-blockit-dest (Invitrogen) was inserted into pLenti-IRES-hrGFP at the site of ClaI and XhoI. This vector was named pLenti-dest-IRES-hrGFP (pLDIG). INAM sequence 5′-CTTCTCTCCG-GTTAGTTATCT-3′ was targeted for INAM knockdown (shINAM/pLDIG) and 5′-AGTCTGACATACTTATACTTA-3′ was used for negative control (shCont/pLDIG). We used a gene-expression kit, Lentiviral system (Invitrogen), as previously described (Akazawa et al., 2007a). Four plasmids (one of the pLenti vectors, pLP1, pLP2, and pLP/VSVG) were transfected into 293 FT packaging cells, and the viral particles for transfection were prepared according to the manufacturer's protocol. The 100× concentrated virus particles were produced after centrifugation of 8,000 *g* at 4°C for 16 h. Lentivirus produced by pLenti-IRES-hrGFP and pLDIBG could be tittered by GFP expression using flow cytometry. Because the lentivirus vector pLenti-IRES-hrGFP has the IRES-GFP region, we prepared negative control virus by pLenti-IRES-hrGFP without construct. Infection efficiency for BMDC was high with the control vector compared with the INAM-expressing lentivector (Fig. S6 A).

Real-time PCR. BMDCs were harvested after 4 h of stimulation by 100 ng/ml LPS, 50 μg/ml polyI:C, 1 μg/ml Pam_3CSK_4 (Pam3), 100 nM mycoplasmal macrophage-activating lipopeptide-2 (Malp-2), 10 μg/ml CpG, and 2,000 IU/ml IFN-α (Ebihara et al., 2007). Mouse tissues (heart, stomach, small intestine, large intestine, lung, brain, muscle, liver, kidney, thymus, and spleen) were collected from C57BL/6. Splenocytes were stained with CD3-PE, CD19-PE, DX5-PE, CD11b-PE, CD11c-FITC, and PDCA1-PE (eBioscience) and sorted by FACSAria (BD). Purity was >98% in each population. For RNA extraction, we used the RNeasy kit (Invitrogen). After removal of genomic DNA by treatment with DNase, randomly primed cDNA strands were generated with Moloney mouse leukemia virus reverse transcription (Promega). RNA expression was quantified by quantitative RT-PCR with gene-specific primers (IL-15 forward, 5′-TTAACTGAGGCTGGCATTCATG-3′; IL-15 reverse, 5′-ACCTACACTGACACAGCCCAAA-3′; INAM forward, 5′-CAACTGCAATGCCACGCTA-3′; INAM reverse, 5′-TCCAACC-GAACACCTGAGACT-3′; β-actin forward, 5′-TTTGCAGCTCCTTC-GTTGC-3′; β-actin reverse, 5′-TCGTCATCCATGGCGAACT-3′; HPRT forward, 5′-GTTGGATACAGGCCAGACTTTGTTG-3′; and HPRT reverse, 5′-GAAGGGTAGGCTGGCCTATAGGCT-3′) and values were normalized to the expression of β-actin mRNA or HPRT mRNA.

Other primers for PCR were designed using Primer Express software (Applied Biosystems) for another experiment. The following primers were used for PCR: β-actin forward, 5′-CCTGGCACCCAGCACAAT-3′ and reverse, 5′-GCCGATCCACACGGAGTACT-3′; granzyme B forward, 5′-TCCTGCTACTGCTGACCTTGTC-3′ and reverse, 5′-ATGATCTC-CCCTGCCTTTGTC-3′; IFN-α4 forward, 5′-CTGCTGGCTGTGAG-GACATACT-3′ and reverse, 5′-AGGCACAGAGGCTGTGTTTCTT-3′; TRAIL (Tnfsf10) forward, 5′-CTTCACCAACGAGATGAAGCAG-3′ and reverse, 5′-TCCGTCTTTGAGAAGCAAGCTA-3′; and IL-12p40 (Il12b), forward, 5′-AATGTCTGCGTGCAAGCTCA-3′ and reverse, 5′-ATGCCCACTTGCTGCATGA-3′.

Anti-INAM pAb. C-terminal INAM (cINAM; 191–314 aa) was subcloned between the NdeI and SalI sites of pColdI vector (Takara Bio Inc.). 6× His-tagged cINAM protein was expressed in BL21 by manufacturer's methods. The cells were sonicated in 20 mM Tris-HCl, 150 mM NaCL, 1 mM PMSF, and 7 M Urea, pH 7.4, on ice. Expression products of cINAM were purified using the HisTrap HP kit (GE Healthcare). The extracted proteins were refolded by stepwise dialysis against decreasing amounts of urea. Rabbit anti-cINAM polyclonal Ab was produced with the cINAM proteins by standard protocol. IgG was purified by precipitation with 33% ammonium sulfate, dialyzed against PBS.

Surface labeling with biotin. Biotinylation of cell surface proteins was performed according to the reported method (Tsuji et al., 2001). In brief, ~10^8 cells were suspended in 1 ml Hepes-buffered saline (HBS), pH 8.5, and incubated with 10 ml of 10 mg/ml NHS-sulfobiotin (Vector Laboratories) for 1 h at room temperature. Cells were washed in HBS three times and then solubilized with lysis buffer containing 1% NP-40, pH 7.4. The cell lysate was immunoprecipitated with avidin-labeled Abs as described previously (Tsuji et al., 2001).

Immunoblot analysis. Lysates were harvested 24 h after transfection of Flag-tagged INAM/pEFBOS into 293FT cells and treated with *N*-glycosidase F

Published November 8, 2010

(PNGaseF; New England Biolabs, Inc.) by the manufacturer's method in some experiments. Protein samples were separated on SDS-PAGE and immunoblotted by anti-Flag M2 Ab (Sigma-Aldrich). In some experiments, we used highly purified rabbit anti–mouse INAM polyclonal Ab for immunoblotting. The anti-INAM IgG was further purified with protein A–Sepharose and absorbed with BL21 bacterial lysate (where the INAM immunogen was produced) that contained no INAM peptide.

Confocal microscopy. BMDCs and NK cells were infected with control or INAM-expressing lentivirus as described previously (Akazawa et al., 2007a). 24 h later, cells were fixed with 4% paraformaldehyde for 30 min and permeabilized with PBS containing 0.5% saponin for 30 min at room temperature. Fixed cells were stained with anti-FLAG mAb and Alexa Fluor 568–conjugated secondary Ab. Stable Ba/F3 transfectants expressing INAM were treated with Cytofix/Cytoperm (BD) according to the manufacturer. Then cells were stained with PE-phalloidin and rabbit anti-INAM pAb followed by Alexa Fluor 488–conjugated secondary Ab. Cells were analyzed on a confocal microscope (LSM 510 META; Carl Zeiss, Inc.) for the detection of INAM.

BMDC–NK interaction. BMDCs were co-cultured with freshly isolated NK cells (BMDC/NK = ~1:2–1:5) with or without 10 μg/ml polyI:C for 24 h (Akazawa et al., 2007a). In some experiments, function of BMDCs and NK cells was modified by lentivirus vector before BMDC/NK co-culture. IRF-3$^{-/-}$ BMDCs were transfected by control lentivirus and INAM-expressing lentivirus (INAM/pLenti-IRES-hrGFP) and incubated with 6 μg/ml polybrene for 24 h before co-culture. WT BMDCs were transfected with shRNA-expressing lentivirus (shCont/pLDIG or shINAM/pLDIG) and incubated with 6 μg/ml polybrene for 48 h before co-culture. Freshly isolated NK cells were transfected with control lentivirus and INAM-expressing lentivirus (INAM/pLenti-IRES-hrGFP) and cultured with 6 μg/ml polybrene in the presence of 500 IU/ml IL-2 for 72 h before co-culture. Activation of NK cells was assessed by concentration of IFN-γ (ELISA; GE Healthcare) in the medium and by NK cytotoxicity against B16D8. Cytotoxicity was determined by standard ^{51}Cr release assay as described previously (Akazawa et al., 2007a).

Ex vivo NK activation. Mice were i.p. injected with 250 μg polyI:C. After 24 h, spleen cells were harvested and then NK cells (DX5$^+$ cells) were positively isolated with the MACS system (Miltenyi Biotec). The DX5$^+$ NK cells were suspended in RPMI1640 with 10% FCS and mixed with ^{51}Cr-labeled B16D8 cells at indicated E/T ratios. After 4 h, supernatants were harvested and ^{51}Cr release was measured. Specific lysis was calculated by (specific release − spontaneous release)/(max release − spontaneous release). In some experiments, blood was drawn from the eyes of mice 8 h after polyI:C administration for cytokine measurement.

Test for in vivo NK activation in LN. 5 × 10^5 WT BMDCs incubated with or without 10 μg/ml polyI:C for 24 h or 5 × 10^5 IRF-3$^{-/-}$ BMDCs infected with control virus or INAM-expressing lentivirus and allowed to stand for 24 h were injected into the footpads of WT C57BL/6 mice. 48 h later, cells in their inguinal LN were harvested, stained with PE-DX5, and sorted by FACSAria II. RNA was extracted from the DX5-positive cells with TRIzol.

DC therapy. DC therapy against mice with B16D8 tumor burden was described previously (Akazawa et al., 2007a). C57BL/6 mice (n = 3) were shaved at the flank and injected s.c. with 6 × 10^5 syngeneic B16D8 melanoma cells (indicated as day 0). For DC therapy, BMDCs were prepared by transfecting control lentivirus or INAM-expressing lentivirus (INAM/pLenti-IRES-hrGFP) and cultured for 24 h. At the time point indicated in the figures, 10^6 BMDCs were injected s.c. near the tumor. To deplete NK cells in vivo, mice were i.p. injected with hybridoma ascites of anti-NK1.1 mAb (PK136; Akazawa et al., 2007a). Tumor volumes were measured using a caliper every 1 or 2 d. Tumor volume was calculated using the formula: tumor volume (cm^3) = (long diameter) × (short diameter) × (short diameter) × 0.4.

Statistical analysis. Statistical analyses were made with the Student's t test. The p-value of significant differences is reported.

Online supplemental material. TICAM-1–inducible genes encoding putative membrane proteins relevant for this study are summarized in Table S1. Fig. S1 shows KO mice results suggesting that both IPS-1 and TICAM-1 in BMDC participate in polyI:C-driven NK activation. Data presented in Fig. S2 characterizes the in vivo polyI:C response of INAM in LN cells. Figs. S3 and S4 demonstrate the properties of surface-expressed INAM analyzed by immunoprecipitation/blotting and confocal microscopy, respectively. Fig. S5 mentions the cytokine expression and maturation profiles of INAM-overexpressing BMDC. Fig. S6 shows the effect of gene silencing of INAM on the polyI:C-mediated cytokine-inducing profile in BMDC. Two pieces of data presented in Fig. S7 confirm the presence of the INAM protein in INAM lentivirus-transduced BMDCs and NK cells. Online supplemental material is available at http://www.jem.org/cgi/content/full/jem.20091573/DC1.

We thank Drs. T. Akazawa and N. Inoue (Osaka Medical Center for Cancer, Osaka, Japan) for their valuable discussions. Thanks are also due to many discussions by our laboratory members. Particularly, extensive English review by Dr. Hussein H. Aly is gratefully acknowledged.

This project was supported by Grants-in-Aid from the Ministry of Education, Science, and Culture and the Ministry of Health, Labor, and Welfare of Japan, Mitsubishi Foundation, Mochida Foundation, NorthTec Foundation Waxman Foundation, and Yakult Foundation.

The authors declare no financial or commercial conflict of interest.

Submitted: 20 July 2009
Accepted: 13 October 2010

REFERENCES

Akazawa, T., T. Ebihara, M. Okuno, Y. Okuda, M. Shingai, K. Tsujimura, T. Takahashi, M. Ikawa, M. Okabe, N. Inoue, et al. 2007a. Antitumor NK activation induced by the Toll-like receptor 3-TICAM-1 (TRIF) pathway in myeloid dendritic cells. *Proc. Natl. Acad. Sci. USA.* 104:252–257. doi:10.1073/pnas.0605978104

Akazawa, T., M. Shingai, M. Sasai, T. Ebihara, N. Inoue, M. Matsumoto, and T. Seya. 2007b. Tumor immunotherapy using bone marrow-derived dendritic cells overexpressing Toll-like receptor adaptors. *FEBS Lett.* 581:3334–3340. doi:10.1016/j.febslet.2007.06.019

Azuma, M., R. Sawahata, Y. Akao, T. Ebihara, S. Yamazaki, M. Matsumoto, M. Hashimoto, K. Fukase, Y. Fujimoto, and T. Seya. 2010. The peptide sequence of diacyl lipopeptides determines dendritic cell TLR2-mediated NK activation. *PLoS One.* 5:e12550. doi:10.1371/journal.pone.0012550

Bertram, L., B.M. Schjeide, B. Hooli, K. Mullin, M. Hiltunen, H. Soininen, M. Ingelsson, L. Lannfelt, D. Blacker, and R.E. Tanzi. 2008. No association between CALHM1 and Alzheimer's disease risk. *Cell.* 135:993–994, author reply :994–996. doi:10.1016/j.cell.2008.11.030

Brandt, C.S., M. Baratin, E.C. Yi, J. Kennedy, Z. Gao, B. Fox, B. Haldeman, C.D. Ostrander, T. Kaifu, C. Chabannon, et al. 2009. The B7 family member B7-H6 is a tumor cell ligand for the activating natural killer cell receptor NKp30 in humans. *J. Exp. Med.* 206:1495–1503. doi:10.1084/jem.20090681

Brilot, F., T. Strowig, S.M. Roberts, F. Arrey, and C. Münz. 2007. NK cell survival mediated through the regulatory synapse with human DCs requires IL-15Ralpha. *J. Clin. Invest.* 117:3316–3329. doi:10.1172/JCI31751

Cerwenka, A., and L.L. Lanier. 2001. Natural killer cells, viruses and cancer. *Nat. Rev. Immunol.* 1:41–49. doi:10.1038/35095564

Cerwenka, A., A.B. Bakker, T. McClanahan, J. Wagner, J. Wu, J.H. Phillips, and L.L. Lanier. 2000. Retinoic acid early inducible genes define a ligand family for the activating NKG2D receptor in mice. *Immunity.* 12:721–727. doi:10.1016/S1074-7613(00)80222-8

Cerwenka, A., J.L. Baron, and L.L. Lanier. 2001. Ectopic expression of retinoic acid early inducible-1 gene (RAE-1) permits natural killer cell-mediated rejection of a MHC class I-bearing tumor in vivo. *Proc. Natl. Acad. Sci. USA.* 98:11521–11526. doi:10.1073/pnas.201238598

Dreses-Werringloer, U., J.C. Lambert, V. Vingtdeux, H. Zhao, H. Vais, A. Siebert, A. Jain, J. Koppel, A. Rovelet-Lecrux, D. Hannequin, et al. 2008. A polymorphism in CALHM1 influences Ca2+ homeostasis,

Abeta levels, and Alzheimer's disease risk. *Cell.* 133:1149–1161. doi:10.1016/j.cell.2008.05.048

Ebihara, T., H. Masuda, T. Akazawa, M. Shingai, H. Kikuta, T. Ariga, M. Matsumoto, and T. Seya. 2007. Induction of NKG2D ligands on human dendritic cells by TLR ligand stimulation and RNA virus infection. *Int. Immunol.* 19:1145–1155. doi:10.1093/intimm/dxm073

Fernandez, N.C., A. Lozier, C. Flament, P. Ricciardi-Castagnoli, D. Bellet, M. Suter, M. Perricaudet, T. Tursz, E. Maraskovsky, and L. Zitvogel. 1999. Dendritic cells directly trigger NK cell functions: cross-talk relevant in innate anti-tumor immune responses in vivo. *Nat. Med.* 5:405–411. doi:10.1038/7403

Fitzgerald, K.A., S.M. McWhirter, K.L. Faia, D.C. Rowe, E. Latz, D.T. Golenbock, A.J. Coyle, S.M. Liao, and T. Maniatis. 2003. IKKepsilon and TBK1 are essential components of the IRF3 signaling pathway. *Nat. Immunol.* 4:491–496. doi:10.1038/ni921

Gerosa, F., B. Baldani-Guerra, C. Nisii, V. Marchesini, G. Carra, and G. Trinchieri. 2002. Reciprocal activating interaction between natural killer cells and dendritic cells. *J. Exp. Med.* 195:327–333. doi:10.1084/jem.20010938

Hamerman, J.A., K. Ogasawara, and L.L. Lanier. 2004. Cutting edge: Toll-like receptor signaling in macrophages induces ligands for the NKG2D receptor. *J. Immunol.* 172:2001–2005.

Honda, K., H. Yanai, H. Negishi, M. Asagiri, M. Sato, T. Mizutani, N. Shimada, Y. Ohba, A. Takaoka, N. Yoshida, and T. Taniguchi. 2005. IRF-7 is the master regulator of type-I interferon-dependent immune responses. *Nature.* 434:772–777. doi:10.1038/nature03464

Hornung, V., S. Rothenfusser, S. Britsch, A. Krug, B. Jahrsdörfer, T. Giese, S. Endres, and G. Hartmann. 2002. Quantitative expression of toll-like receptor 1-10 mRNA in cellular subsets of human peripheral blood mononuclear cells and sensitivity to CpG oligodeoxynucleotides. *J. Immunol.* 168:4531–4537.

Huntington, N.D., N. Legrand, N.L. Alves, B. Jaron, K. Weijer, A. Plet, E. Corcuff, E. Mortier, Y. Jacques, H. Spits, and J.P. Di Santo. 2009. IL-15 trans-presentation promotes human NK cell development and differentiation in vivo. *J. Exp. Med.* 206:25–34. doi:10.1084/jem.20082013

Iwasaki, A., and R. Medzhitov. 2004. Toll-like receptor control of the adaptive immune responses. *Nat. Immunol.* 5:987–995. doi:10.1038/ni1112

Kalinski, P., R.B. Mailliard, A. Giermasz, H.J. Zeh, P. Basse, D.L. Bartlett, J.M. Kirkwood, M.T. Lotze, and R.B. Herberman. 2005. Natural killer-dendritic cell cross-talk in cancer immunotherapy. *Expert Opin. Biol. Ther.* 5:1303–1315. doi:10.1517/14712598.5.10.1303

Kato, H., O. Takeuchi, S. Sato, M. Yoneyama, M. Yamamoto, K. Matsui, S. Uematsu, A. Jung, T. Kawai, K.J. Ishii, et al. 2006. Differential roles of MDA5 and RIG-I helicases in the recognition of RNA viruses. *Nature.* 441:101–105. doi:10.1038/nature04734

Kawai, T., K. Takahashi, S. Sato, C. Coban, H. Kumar, H. Kato, K.J. Ishii, O. Takeuchi, and S. Akira. 2005. IPS-1, an adaptor triggering RIG-I- and Mda5-mediated type I interferon induction. *Nat. Immunol.* 6:981–988. doi:10.1038/ni1243

Kubin, M.Z., D.L. Parshley, W. Din, J.Y. Waugh, T. Davis-Smith, C.A. Smith, B.M. Macduff, R.J. Armitage, W. Chin, L. Cassiano, et al. 1999. Molecular cloning and biological characterization of NK cell activation-inducing ligand, a counterstructure for CD48. *Eur. J. Immunol.* 29:3466–3477. doi:10.1002/(SICI)1521-4141(199911)29:11<3466::AID-IMMU3466>3.0.CO;2-9

Lee, A.E., L.A. Rogers, J.M. Longcroft, and R.E. Jeffery. 1990. Reduction of metastasis in a murine mammary tumour model by heparin and polyinosinic-polycytidylic acid. *Clin. Exp. Metastasis.* 8:165–171. doi:10.1007/BF00117789

Levy, S., and T. Shoham. 2005. The tetraspanin web modulates immune-signalling complexes. *Nat. Rev. Immunol.* 5:136–148. doi:10.1038/nri1548

Lucas, M., W. Schachterle, K. Oberle, P. Aichele, and A. Diefenbach. 2007. Dendritic cells prime natural killer cells by trans-presenting interleukin 15. *Immunity.* 26:503–517. doi:10.1016/j.immuni.2007.03.006

Masuda, H., Y. Saeki, M. Nomura, K. Shida, M. Matsumoto, M. Ui, L.L. Lanier, and T. Seya. 2002. High levels of RAE-1 isoforms on mouse tumor cell lines assessed by anti-"pan" RAE-1 antibody confer tumor susceptibility to NK cells. *Biochem. Biophys. Res. Commun.* 290:140–145. doi:10.1006/bbrc.2001.6165

Matsumoto, M., and T. Seya. 2008. TLR3: interferon induction by double-stranded RNA including poly(I:C). *Adv. Drug Deliv. Rev.* 60:805–812. doi:10.1016/j.addr.2007.11.005

McCartney, S., W. Vermi, S. Gilfillan, M. Cella, T.L. Murphy, R.D. Schreiber, K.M. Murphy, and M. Colonna. 2009. Distinct and complementary functions of MDA5 and TLR3 in poly(I:C)-mediated activation of mouse NK cells. *J. Exp. Med.* 206:2967–2976. doi:10.1084/jem.20091181

Medzhitov, R., and C.A. Janeway Jr. 1997. Innate immunity: the virtues of a nonclonal system of recognition. *Cell.* 91:295–298. doi:10.1016/S0092-8674(00)80412-2

Meylan, E., J. Curran, K. Hofmann, D. Moradpour, M. Binder, R. Bartenschlager, and J. Tschopp. 2005. Cardif is an adaptor protein in the RIG-I antiviral pathway and is targeted by hepatitis C virus. *Nature.* 437:1167–1172. doi:10.1038/nature04193

Miyake, T., Y. Kumagai, H. Kato, Z. Guo, K. Matsushita, T. Satoh, T. Kawagoe, H. Kumar, M.H. Jang, T. Kawai, et al. 2009. Poly I:C-induced activation of NK cells by CD8 alpha+ dendritic cells via the IPS-1 and TRIF-dependent pathways. *J. Immunol.* 183:2522–2528. doi:10.4049/jimmunol.0901500

Mukai, M., F. Imamura, M. Ayaki, K. Shinkai, T. Iwasaki, K. Murakami-Murofushi, H. Murofushi, S. Kobayashi, T. Yamamoto, H. Nakamura, and H. Akedo. 1999. Inhibition of tumor invasion and metastasis by a novel lysophosphatidic acid (cyclic LPA). *Int. J. Cancer.* 81:918–922. doi:10.1002/(SICI)1097-0215(19990611)81:6<918::AID-IJC13>3.0.CO;2-E

Newman, K.C., and E.M. Riley. 2007. Whatever turns you on: accessory-cell-dependent activation of NK cells by pathogens. *Nat. Rev. Immunol.* 7:279–291. doi:10.1038/nri2057

Nomura, M., Z. Zou, T. Joh, Y. Takihara, Y. Matsuda, and K. Shimada. 1996. Genomic structures and characterization of Rae1 family members encoding GPI-anchored cell surface proteins and expressed predominantly in embryonic mouse brain. *J. Biochem.* 120:987–995.

Ohteki, T., H. Tada, K. Ishida, T. Sato, C. Maki, T. Yamada, J. Hamuro, and S. Koyasu. 2006. Essential roles of DC-derived IL-15 as a mediator of inflammatory responses in vivo. *J. Exp. Med.* 203:2329–2338. doi:10.1084/jem.20061297

Oshiumi, H., M. Matsumoto, K. Funami, T. Akazawa, and T. Seya. 2003a. TICAM-1, an adaptor molecule that participates in Toll-like receptor 3-mediated interferon-beta induction. *Nat. Immunol.* 4:161–167. doi:10.1038/ni886

Oshiumi, H., M. Sasai, K. Shida, T. Fujita, M. Matsumoto, and T. Seya. 2003b. TIR-containing adapter molecule (TICAM)-2, a bridging adapter recruiting to toll-like receptor 4 TICAM-1 that induces interferon-beta. *J. Biol. Chem.* 278:49751–49762. doi:10.1074/jbc.M305820200

Sasai, M., M. Shingai, K. Funami, M. Yoneyama, T. Fujita, M. Matsumoto, and T. Seya. 2006. NAK-associated protein 1 participates in both the TLR3 and the cytoplasmic pathways in type I IFN induction. *J. Immunol.* 177:8676–8683.

Sato, M., H. Suemori, N. Hata, M. Asagiri, K. Ogasawara, K. Nakao, T. Nakaya, M. Katsuki, S. Noguchi, N. Tanaka, and T. Taniguchi. 2000. Distinct and essential roles of transcription factors IRF-3 and IRF-7 in response to viruses for IFN-alpha/beta gene induction. *Immunity.* 13:539–548. doi:10.1016/S1074-7613(00)00053-4

Seth, R.B., L. Sun, C.K. Ea, and Z.J. Chen. 2005. Identification and characterization of MAVS, a mitochondrial antiviral signaling protein that activates NF-kappaB and IRF 3. *Cell.* 122:669–682. doi:10.1016/j.cell.2005.08.012

Seya, T., and M. Matsumoto. 2009. The extrinsic RNA-sensing pathway for adjuvant immunotherapy of cancer. *Cancer Immunol. Immunother.* 58:1175–1184. doi:10.1007/s00262-008-0652-9

Sivori, S., M. Falco, M. Della Chiesa, S. Carlomagno, M. Vitale, L. Moretta, and A. Moretta. 2004. CpG and double-stranded RNA trigger human NK cells by Toll-like receptors: induction of cytokine release and cytotoxicity against tumors and dendritic cells. *Proc. Natl. Acad. Sci. USA.* 101:10116–10121. doi:10.1073/pnas.0403744101

Tanaka, H., Y. Mori, H. Ishii, and H. Akedo. 1988. Enhancement of metastatic capacity of fibroblast-tumor cell interaction in mice. *Cancer Res.* 48:1456–1459.

Tsuji, S., J. Uehori, M. Matsumoto, Y. Suzuki, A. Matsuhisa, K. Toyoshima, and T. Seya. 2001. Human intelectin is a novel soluble lectin that recognizes galactofuranose in carbohydrate chains of bacterial cell wall. *J. Biol. Chem.* 276:23456–23463. doi:10.1074/jbc.M103162200

Vivier, E., E. Tomasello, M. Baratin, T. Walzer, and S. Ugolini. 2008. Functions of natural killer cells. *Nat. Immunol.* 9:503–510. doi:10.1038/ni1582

Xu, L.G., Y.Y. Wang, K.J. Han, L.Y. Li, Z. Zhai, and H.B. Shu. 2005. VISA is an adapter protein required for virus-triggered IFN-beta signaling. *Mol. Cell.* 19:727–740. doi:10.1016/j.molcel.2005.08.014

Yamamoto, M., S. Sato, H. Hemmi, K. Hoshino, T. Kaisho, H. Sanjo, O. Takeuchi, M. Sugiyama, M. Okabe, K. Takeda, and S. Akira. 2003a. Role of adaptor TRIF in the MyD88-independent toll-like receptor signaling pathway. *Science.* 301:640–643. doi:10.1126/science.1087262

Yamamoto, M., S. Sato, H. Hemmi, S. Uematsu, K. Hoshino, T. Kaisho, O. Takeuchi, K. Takeda, and S. Akira. 2003b. TRAM is specifically involved in the Toll-like receptor 4-mediated MyD88-independent signaling pathway. *Nat. Immunol.* 4:1144–1150. doi:10.1038/ni986

Yoneyama, M., M. Kikuchi, T. Natsukawa, N. Shinobu, T. Imaizumi, M. Miyagishi, K. Taira, S. Akira, and T. Fujita. 2004. The RNA helicase RIG-I has an essential function in double-stranded RNA-induced innate antiviral responses. *Nat. Immunol.* 5:730–737. doi:10.1038/ni1087

Zanoni, I., M. Foti, P. Ricciardi-Castagnoli, and F. Granucci. 2005. TLR-dependent activation stimuli associated with Th1 responses confer NK cell stimulatory capacity to mouse dendritic cells. *J. Immunol.* 175:286–292.

Zou, Z., M. Nomura, Y. Takihara, T. Yasunaga, and K. Shimada. 1996. Isolation and characterization of retinoic acid-inducible cDNA clones in F9 cells: a novel cDNA family encodes cell surface proteins sharing partial homology with MHC class I molecules. *J. Biochem.* 119:319–328.